Fat1 deletion promotes hybrid EMT state with enhanced tumor progression, stemness, and metastasis

Ievgenia Pastushenko[1,2,3*], Federico Mauri[1*], Yura Song[1], Florian de Cock[1], Bob Meeusen[4,5], Benjamin Swedlund[1], Francis Impens[6], Delphi Van Haver[6], Matthieu Optiz[7], Manuel Thery[8,9], Yacine Bareche[10], Gaelle Lapouge[1], Marjorie Vermeersch[11], Yves-Rémi Van Eycke[12,13], Cédric Balsat[12], Christine Decaestecker[12,13], Youri Sokolow[14], Sergio Hassid[15], Alicia Perez-Bustillo[16], Beatriz Agreda-Moreno[17], Luis Rios-Buceta[18], Pedro Jaen[18], Pedro Redondo[19], Ramon Sieira-Gil[20], Jose F. Millan-Cayetano[21], Onofre Sanmatrtin[22], Nicky D'Haene[23], Virginie Moers[1], Milena Rozzi[1], Jeremy Blondeau[1], Sophie Lemaire[1], Samuel Scozzaro[1], Christine Dubois[1], David Pérez-Morga[11,24], Isabelle Salmon[23], Christos Sotiriou[10], Francoise Helmbacher[25] and Cédric Blanpain[1,26,27]

1. Université libre de Buxelles (ULB), Laboratory of Stem Cells and Cancer, 808 route de Lennik, 1070 Brussels, Belgium
2. Dermatology Department, Cliniques de l'Europe, Bruxelles, Belgium
3. Dermatology Department, CHU Brugmann, Université Libre de Bruxelles, Belgium.
4. Laboratory of Protein Phosphorylation & Proteomics, Dept. of Cellular & Molecular Medicine, KU Leuven, Leuven, Belgium.
5. Leuven Cancer Institute (LKI), Leuven, Belgium.
6. VIB Center for Medical Biotechnology, VIB Proteomics Core, Department of Biomolecular Medicine, Ghent University, Ghent, Belgium
7. Alvéole, 68 Boulevard de Port-Royal, 75005, Paris, France
8. Université de Paris, CEA/ INSERM/AP-HP, Institut de Recherche Saint Louis, UMR976, HIPI, CytoMorpho Lab, Hopital Saint Louis, 1 Avenue Claude Vellefaux, 75010 Paris, France
9. Université Grenoble-Alpes, CEA/INRA/CNRS, Interdisciplinary Research Institute of Grenoble, UMR5168, LPCV, CytoMorpho Lab, 17 rue des Martyrs, 38054 Grenoble, France
10. Breast Cancer Translational Research Laboratory, J.-C. Heuson, Institut Jules Bordet, Université Libre de Bruxelles, Brussels, Belgium
11. Center for Microscopy and Molecular Imaging (CMMI), Université Libre de Bruxelles, 12, rue des Profs Jeener et Brachet, B-6041 Gosselies, Belgium

12. DIAPath, Center for Microscopy and Molecular Imaging, Université Libre de Bruxelles (ULB), CPI 305/1, Rue Adrienne Bolland, 8, 6041 Gosselies
13. Laboratory of Image Synthesis and Analysis, Ecole Polytechnique de Bruxelles, ULB, 1050 Brussels, Belgium
14. Thoracic Surgery, Erasme University Hospital, Universite Libre de Bruxelles, Brussels B-1070, Belgium
15. Department of Otolaryngology-Head and Neck Surgery, Erasme Hospital, Route de Lennik 808, 1070 Brussels, Belgium
16. Department of Dermatology, Complejo Asistencial de Leon, Leon, Spain.
17. Department of Otolaryngology – Head and Neck Surgery, Hospital Clinico "Lozano Blesa", Zaragoza, Spain.
18. Dermatology Department, Ramón y Cajal Hospital Madrid, Spain. University of Alcalá, Madrid, Spain.
19. Department of Dermatology, Clinica Universidad de Navarra, Navarra, Spain
20. Department of Otolaryngology – Head and Neck Surgery, Hospital Clinic, Barcelona, Spain
21. Department of Dermatology, Hospital Costa del Sol, Marbella, Spain
22. Department of Dermatology, Instituto Valenciano de Oncologia, Valencia, Spain.
23. Pathology Department, Erasme Hospital, Université Libre de Bruxelles, Brussels B-1070, Belgium
24. Laboratory of Molecular Parasitology, IBMM, Université Libre de Bruxelles, 12, rue des Profs Jeener et Brachet, B6041 Gosselies, Belgium
25. Aix-Marseille University, CNRS, IBDM, UMR 7288, Case 907 Parc Scientifique de Luminy, 13288 Marseille Cedex 9 France
26. WELBIO, Université Libre de Bruxelles (ULB), 1070 Bruxelles, Belgium
27. Corresponding author: Cedric.Blanpain@ulb.ac.be

*These authors contributed equally to this work

***Fat1*, a protocadherin, is among the most frequently mutated genes in human cancers. However, the role and the molecular mechanisms by which *Fat1* mutation controls tumor initiation and progression are poorly understood. Here, using different mouse cancer models including skin squamous cell carcinoma (SCC) and lung tumors, we found that *Fat1* deletion (*Fat1cKO*) accelerated tumor appearance, increased the number of tumors and their malignant transition. *Fat1cKO* carcinomas were much more invasive and presented hybrid epithelial to mesenchymal (EMT) features. This hybrid EMT state was also found in *FAT1* mutated human SCCs. *Fat1cKO* skin SCCs presented increased tumor stemness and spontaneous metastasis. Transcriptional and chromatin profiling identified a mutated *FAT1* signature, which is associated with poor prognosis. Proteomic analyses and mechanistic studies revealed that *FAT1* loss of function activates a CAMK2/CD44/SRC axis that promotes YAP/ZEB1 nuclear translocation and stimulates the mesenchymal state, as well as a CAMK2-EZH2 axis that promotes activation of SOX2, which sustains the epithelial state. This comprehensive analysis also identified drug resistance and vulnerabilities in *FAT1* deficient tumors with important implications for cancer therapy. Altogether, our studies revealed that *Fat1* loss of function promotes tumor initiation, progression, invasiveness, stemness and metastasis through the induction of a hybrid EMT state.**

Introduction

FAT1 is very frequently mutated in a broad range of human cancers, in particular in squamous cell carcinomas (SCCs) originating from various body locations including skin, head and neck, oesophagus and lung [1-10]. Mutations in *FAT1* have been associated with poor clinical outcome in patients with cancers and resistance to therapy in breast cancer [11-14]. In the most frequently used cancer mouse model, the chemical carcinogen (DMBA/TPA) induced skin SCCs, *Fat1* is mutated in about 20% of the cases, as in human SCCs [15]. Stop-gain mutations are very frequently found, indicating that these mutations most likely result in loss-of-function (LOF) and that *FAT1* acts as a tumor suppressor gene (TSG). ShRNA mediated knock-down of *FAT1* in human cancer cell lines decreased cell-cell adhesion and promoted cell migration, whereas contradictory results were obtained on the role of *FAT1* in regulating Epithelial to Mesenchymal Transition (EMT) in cancer cell lines *in vitro* [16-20]. However, the formal *in-vivo* demonstration that *Fat1* indeed acts as a TSG by genetic LOF experiment is still lacking. More importantly, the molecular mechanisms by which *FAT1* mutation promotes tumorigenesis and controls tumor heterogeneity *in vivo* are completely unknown.

Fat1 **deletion promotes tumorigenesis and malignant progression**

To assess whether *Fat1* LOF promotes tumor initiation, we performed conditional deletion of *Fat1* in the skin epidermis using the constitutive *K14CRE* (*K14-CRE/Fat1$^{flox/flox}$/Rosa26$^{YFP/+}$* referred to as *Fat1cKO*). *K14-Fat1cKO* mice were born at a Mendelian ratio and were viable without any macroscopic abnormalities in the skin or other squamous epithelia expressing the *K14CRE* (Extended Data 1a,b). The skin epidermis in *Fat1cKO* mice was microscopically undistinguishable from controls in homeostatic conditions (Extended Data 1c-e). Following chemically-induced skin carcinogenesis

(DMBA/TPA administration), tumorigenesis developed more rapidly and the number of skin tumors per mouse was markedly increased in *Fat1cKO* mice (Fig. 1a-d), demonstrating formally and rigorously that *Fat1* acts a TSG in chemical carcinogen induced skin SCCs.

To determine whether *Fat1* LOF promotes tumor progression, we first assessed macroscopically the number of benign papillomas per mouse that progressed spontaneously into malignant SCCs, recognized morphologically by the macroscopic appearance of carcinoma features (Fig. 1e). The number of SCCs was increased in *Fat1cKO* mice (Fig. 1f), suggesting that *Fat1* may also restrict tumor progression. However, due to the different timing of tumor appearance, growth rate, and number of tumors per mouse, it is difficult to draw from these experiments definitive conclusions about the precise role of *Fat1* during malignant progression. To address this question in a more direct and controlled manner, we assessed the rate of malignant progression upon acute deletion of *Fat1* in pre-existing papillomas. To this end, we treated with tamoxifen *K14-CREER/Fat1*$^{flox/flox}$*/Rosa26*$^{YFP/+}$ mice already bearing DMBA/TPA induced skin papillomas, inducing the acute deletion of *Fat1* in benign skin tumors (Fig. 1g). A much higher proportion of benign skin tumors macroscopically progressed into invasive SCCs upon acute *Fat1* deletion (Fig. 1h-i), clearly showing the importance of *Fat1* LOF in promoting malignant progression. To get better insights into the temporality and cellular mechanisms of malignant progression induced by *Fat1* deletion, we characterized microscopically the changes in histology and markers expression over time after acute deletion of *Fat1* in benign papillomas. As soon as 2 weeks following *Fat1* deletion, the shape of the cells of the papillomas changed, the basal lamina as shown by Lam5 immunostaining was discontinued and K10 expression, characteristic of benign tumors, was decreased (Fig. 1j,k). After 4 weeks following tamoxifen administration, the shape of the cells was even more irregular, almost no K10 expressing cells were present

and Lam5 expression was discontinued (Fig. 1j,k). These data indicate that malignant progression occurs very rapidly upon *Fat1* deletion.

The changes in cell behaviour observed following *Fat1* deletion prompted us to investigate whether *Fat1* controls cell polarity and cell adhesion. Immunostaining analysis indicated that classical polarity and adhesion markers such as E-Cadherin, Zo-1 or Cldn-1, were all strongly decreased in *Fat1cKO* papillomas (Fig. 1l). Electron Microscopy (EM) of *Fat1cKO* papillomas confirmed the loss of polarity (Fig.1 m) and showed that whereas the number and the structure of desmosomes were unaffected, the adherens and tight junctions were no longer observed in *Fat1cKO* papillomas (Fig. 1n-p). Consistently with the decrease in Lam5 expression, EM analysis revealed fenestration of the basal lamina and a decrease in the number of hemidesmosomes in *Fat1cKO* tumors (Fig 1q,r). These data demonstrate that *Fat1* controls the attachment of the cells to the stroma, cell polarity and cell adhesion between tumor cells.

Fat1 **deletion promotes hybrid EMT**

These histological differences persisted in malignant SCCs. *Fat1cKO* SCCs were less cohesive, with rounded cell shapes, and with most cells expressing the mesenchymal marker Vimentin, suggesting that they underwent EMT (Fig. 2a). We have recently identified distinct tumour EMT transition states characterized by expression of different levels of the cell surface markers Epcam/CD106/CD61/CD51 and representing different stages within the EMT process, ranging from epithelial state, epithelial and mesenchymal hybrid state to fully mesenchymal state [21]. FACS analysis of *Fat1cKO* SCCs showed that *Fat1* deletion was associated with EMT, as *Fat1* mutated tumors contained an important proportion of cells that lost Epcam expression, which was very rare in *Fat1* WT DMBA/TPA SCCs (Fig. 2b,c). EMT occurred very early during tumor progression, as Epcam- TCs could be detected in tumors

that macroscopically appeared as papillomas (Extended Data 1f), and while both Epcam+ and Epcam- *Fat1cKO* cells expressed high levels of epithelial genes (e.g. E-cadherin, Krt14 or p63), Epcam- *Fat1cKO* papillomas cells expressed high levels of mesenchymal genes such as Vim, Zeb1 or Twist1, among others (Extended Data 1g,h). These data clearly demonstrate that *Fat1* LOF dramatically accelerates malignant progression. The majority of the Epcam- EMT TCs were negative for CD106/CD61/CD51 markers or expressed CD106 alone (Fig. 2d, Extended Data 2a,b), two hybrid EMT subpopulations characterized by the co-expression of epithelial and mesenchymal markers in genetically induced skin SCCs [21]. To further substantiate that *Fat1* deletion promotes the appearance of hybrid EMT state during tumorigenesis, we isolated YFP+Epcam+ and YFP+Epcam- TCs by FACS and performed immunostaining of K14 and Vimentin on cytospin of the different tumor subpopulations. Similarly to the situation found in genetically induced SCCs presenting EMT [21], *Fat1* deletion in DMBA/TPA-induced SCCs promoted the appearance of hybrid EMT subpopulations co-expressing epithelial and mesenchymal markers (Fig. 2e,f). These data clearly demonstrate, for the first time, that a genetic mutation in a TSG can promote the acquisition of a stable hybrid EMT phenotype.

To assess whether loss of *Fat1* promotes the acquisition of the hybrid EMT phenotype in other mouse cancer models, we combined the *Fat1* floxed alleles with two other genetically engineered skin SCC models induced by $KRas^{G12D}$ expression and *p53* deletion in different epidermal lineages, associated with low and high EMT tumors. *K14-CREER,* targeting the interfollicular epidermis (IFE), induces SCCs with well differentiated phenotypes without EMT features, whereas *Lgr5CREER*, targeting hair follicle (HF) cells, induces heterogeneous tumors characterized by different degrees of EMT, ranging from well differentiated to completely mesenchymal tumors[22]. Similarly to what we found in DMBA/TPA derived SCCs, loss of *Fat1* in the

K14CREER/KRas^{G12D}/p53^{cKO}/Fat1^{cKO}/Rosa26$^{YFP/+}$ model promoted the acquisition of hybrid EMT features with all Epcam- TC populations characterized by the hybrid phenotypes including CD106/CD61/CD51 triple negative and CD106^{+} populations that co-expressed K14 and Vimentin (Extended Data 3a-f). *Lgr5-CREER* induced SCCs, which presented high proportion of EMT independently of *Fat1* deletion, did not further increase EMT features upon *Fat1* LOF. Interestingly, and in contrast with the control condition [21], most TCs continued to express K14 and presented signs of squamous differentiation visible as keratin pearls (Extended data 3g-m). These data demonstrate that in three independent mouse models of primary SCC, *Fat1* deletion specifically promotes the acquisition of stable hybrid EMT phenotypes.

To assess whether the promotion of tumor hybrid state by *Fat1* deletion is skin specific or whether it is conserved across different tumor types, we induced *Fat1* deletion together with *KRasG12D* expression and *p53* deletion in the lung epithelia by intra-tracheal instillation of *CRE* expressing adenovirus [23]. *Fat1* deletion massively increased the number of tumors per lung (Extended Data 3n,o) and those tumors also presented signs of hybrid EMT with increased vimentin expression and loss of Epcam in a fraction of tumor cells (Fig. 2g-l). Interestingly, whereas *KRasG12D* expression and *p53* deletion promoted the onset of adenocarcinomas (ADC) characterized by Nkx2-1/TTF-1 expression, the simultaneous deletion of *Fat1* promoted the formation of lung SCCs, characterized by a decreased expression of Nkx2-1/TTF-1 and an increased expression of Sox2 (Fig. 2g). This is consistent with the higher proportion of *FAT1* mutations in lung SCCs [8,9] and suggests that *FAT1* mutations could be a driving force for the acquisition of the squamous tumor phenotype.

To assess the human relevance of our findings, we performed *FAT1* deletion using CRISPR/Cas9 in the A388 human skin SCC cell line, that does not present signs of EMT and in which *FAT1* is not mutated [24]. Interestingly, *FAT1* disruption in human SCC cells triggered

a change in cell morphology, resulting in less cohesive and more round-shaped cells, associated with a decrease of E-cadherin and Claudin-1 expression, and the co-expression of epithelial markers (Keratin 14, p63 and Sox2) with mesenchymal markers (Vimentin and Zeb1) (Fig. 2m), reminiscent of the EMT hybrid state found in mouse SCCs. To further validate the link between *FAT1* mutations in human cancers and the acquisition of a hybrid EMT phenotype, we performed Whole Exome Sequencing of patient derived xenotransplantation of SCCs from different organs and identified SCCs with and without *FAT1* mutation. Co-immunostaining of Pan-cytokeratin and Vimentin showed that *FAT1* mutated SCCs exhibit a much higher EMT hybrid score (defined by the proportion of Pan-cytokeratin/Vimentin double positive cells) as compared to *FAT1* WT SCCs (Fig. 2n,o, Extended Data 4a-c). These data show that *FAT1* mutations promote the acquisition of hybrid EMT state in human cancers.

Fat1 **deletion promotes tumor stemness and metastasis**

EMT has been associated with an increase in tumor stemness following the transplantation of TCs into immunodeficient mice [21,22,25-29]. To assess whether *Fat1* deletion promotes tumor stemness in mouse skin SCC TCs, we performed tumor transplantation assays of FACS-isolated WT and *Fat1cKO* Epcam+ and Epcam- TCs and quantified tumor propagating cell (TPC) frequency. As previously shown [30], the TPC frequency of WT Epcam+ DMBA/TPA SCCs was low (1/4000 TCs). In contrast, the TPC frequency of all (Epcam+ and Epcam-) *Fat1cKO* TCs was dramatically increased (1/100) (Fig. 3a). To assess whether the increase in TPC frequency in *Fat1cKO* SCCs was due to the presence of Epcam- EMT TCs, we transplanted only Epcam+ *Fat1cKO* TCs. We found that the TPC frequency of *Fat1cKO* Epcam+ TCs was 1/600, about 10 fold more clonogenic as compared to their WT counterpart (Fig. 3a). The histology of the secondary tumors following the transplantation of

Epcam+ *Fat1cKO* TCs recapitulated the histology of the primary tumors (Fig. 3b). Tumor stemness is also associated with an increased clonogenicity *in vitro* [31]. To validate our finding using another functional assay, we assessed the clonogenicity of WT and *FAT1* CRISPR/Cas9 knockout (KO) human SCC cell line in 3D tumor spheroid assays. *FAT1* KO cell lines grew much better as compared to their isogenic WT control cell line (Fig. 3c,d). Altogether, these data show that *Fat1* deletion promotes tumor stemness in mouse and human cancers.

Overexpression of Twist1, which promotes EMT, has been shown to increase metastasis in skin SCCs [32]. Furthermore, EMT hybrid tumor state has been associated with the presence of circulating tumor cells and with increased metastatic potential upon intravenous injection of TCs [21]. To assess whether *Fat1* deletion is associated with increased incidence of spontaneous metastasis, we investigated the number of the lymph node (LN) and lung metastasis arising in WT and *Fat1cKO* mice presenting SCCs. Strikingly, the proportion of the mice presenting LN and lung metastases and the number of metastases per mice were increased in mice presenting *Fat1cKO* SCCs (Fig. 3e-h). To assess whether *Fat1cKO* TCs present increased extravasation capacity and lung colonization potential independently of the number of primary SCCs per mouse or of the occurrence of EMT in the tumors, we assessed the ability of Epcam+ FACS-isolated TCs from WT or *Fat1cKO* SCCs to give rise to lung metastases 40 days after intravenous injection. The number of mice with lung metastases and the number of metastases per lung were also strongly increased upon injection of *Fat1cKO* Epcam+ TCs (Fig. 3i-l). These data revealed that *Fat1* LOF greatly increases spontaneous metastasis and lung colonization in skin SCCs.

Transcriptional landscape of *Fat1* mutated tumors

To investigate the molecular mechanisms by which *Fat1* LOF promotes hybrid EMT state, we first explored the transcriptional and chromatin landscape of Epcam+ and Epcam- TCs from WT and *Fat1cKO* mouse skin SCCs. To this end, we FACS purified YFP+ Epcam+ and Epcam- TCs from WT and *Fat1cKO* SCCs and performed RNA-seq and ATAC-seq of these different TC populations. RNA-seq analyses revealed that *Fat1cKO* Epcam+ TCs compared to WT Epcam+ TCs were characterized by a strong upregulation of all the well-known EMT markers and effectors including *Cdh11*, *Pdgfra*, *Fap*, *Vim*, *Lox*, Mmps, *Snai1*, *Prrx1*, *Twist1*, *Zeb1/2*, although the expression of these genes was further upregulated in Epcam- *Fat1KO* TCs as compared to Epcam+ *Fat1KO* TCs (Fig. 4a). The strong upregulation of EMT markers in Epcam+ *Fat1cKO* TCs compared to WT suggests that Epcam+ *Fat1cKO* TCs are already transcriptionally primed to undergo EMT. Although already expressing many EMT TFs, Epcam+ *Fat1cKO* TCs continued to express epithelial markers such as *Epcam*, *Cdh1*, *Krt14*, *Cldn4*, *Dsc2*, *Grhl1/3* and the epithelial splicing factors *Essrp1/2* at a similar level as in WT Epcam+ TCs (Fig. 4b). As expected, Epcam- *Fat1cKO* TCs exhibited a decrease in the expression of several epithelial genes such as *Epcam*, *Cdh1*, *Dsg2*, *Ocln*, *Lama3*, *Ovol1*, *Grhl2* and *Grhl3* (Fig. 4b). However, and in contrast to Epcam- TC from *Lgr5CREER/KRas^{G12D}/p53^{cKO}* derived SCCs, presenting full EMT, Epcam- *Fat1cKO* TCs continued to express several epithelial genes such as *Krt14*, *Cldn4*, *Dsc2*, *Grhl1/3*, *Trp63*, *Sox2* or *Esrp1/2* at a relatively high level (Fig. 4b). The transcriptional signature of Epcam- and Epcam+ *Fat1cKO* TCs overlapped greatly and very significantly with the hybrid signature obtained by RNA-seq of CD106/CD61/CD51 triple negative (TN) hybrid EMT TC populations from *Lgr5CREER/KRas^{G12D}/p53^{cKO}* SCCs that has been recently identified and did not overlap significantly with a late EMT signature (TP vs TN) [21] (Fig. 4c,d). RNAseq from Epcam+ and Epcam- lung cells deleted for *Fat1* and from CRISPR/Cas9 *FAT1* KO human SCC line displayed the upregulation of a similar

mesenchymal gene expression profile including *Zeb1*, *Zeb2* and *Vimentin* following *Fat1* deletion (Fig. 4e,f), uncovering a common gene signature associated with *Fat1* deletion across different tumor types and between mouse and human cancers. Very importantly, high expression of the common RNA mesenchymal signature between mouse skin and lung *Fat1cKO* SCC and human *FAT1* KO SCC was associated with poor overall survival in patients with lung SCC. This common Fat1 signature was associated with the presence of *FAT1* point mutations with variant allelic frequency of more than 20% and with *FAT1* deletion (Fig. 4g, Extended Data 4d,e). Altogether, these data demonstrate that Epcam+ *Fat1cKO* TCs are transcriptionally primed to undergo EMT during tumorigenesis, and following EMT, *Fat1cKO* Epcam- TCs are stabilized in a hybrid EMT state associated with poor survival in lung cancer.

Yap1 and Sox2 regulate mesenchymal and epithelial states downstream of *Fat1* deletion

To define the changes in the chromatin landscape responsible for the transcriptional priming of hybrid EMT state that occurs following *Fat1* deletion, we performed ATAC-seq on FACS-isolated WT and *Fat1cKO* Epcam+ and Epcam- TC populations. We found enhancers within key EMT TFs such as *Zeb1*, *Snail1* and *Twist2* and other EMT markers (e.g. *Vim*, *Col6a3* and others) that are already more accessible in Epcam+ *Fat1cKO* TCs as compared to WT Epcam+ TCs (Extended Data 5a), potentially accounting for the epigenetic priming of EMT upon *Fat1* deletion. We found enhancers that get opened only in Epcam- *Fat1cKO* as compared to Epcam+, and which are associated with progression in EMT, such as in the regulatory regions of *Prrx1*, *Nfatc1*, *Pdgfrb* or *Vcam1/CD106* (Extended Data 5b). To define the TFs responsible for the chromatin priming of EMT in Epcam+ *Fat1cKO* cells, we performed motif discovery analysis of the ATAC-seq peaks that were more opened in Epcam+ *Fat1cKO* TCs as compared to Epcam+ WT TCs. We found that motifs for *AP1*, *Nfi*,

Runx, *Mafk*, *Tead*, *Nfkb* TFs were strongly statistically enriched in the chromatin regions of *Fat1cKO* Epcam+ TCs (Extended Data 5c), suggesting that the Jun/Fos family of TFs cooperates with other TFs including those of the TEAD family, that relay the Yap1 pathway to the nucleus (Fig. 4h,i) to prime the *Fat1* mutated cancer cells to undergo EMT in skin SCC *in vivo* [33,34].

To define the chromatin regions responsible for the hybrid EMT states and for the sustained expression of some epithelial genes in Epcam- Fat1cKO TCs, we investigated the chromatin landscape of the regulatory regions of pro-epithelial TFs. Consistent with their expression changes, we found that many enhancers located in the regulatory regions of pro-epithelial TFs such as *Cebpa*, *Cebpb*, *Grhl1*, *Sox2*, *Klf4* or *AP2g* were still opened in Epcam- *Fat1cKO* TCs, whereas these enhancers were completely closed in Epcam- TCs from *Lgr5CREER/KRas^{G12D}/p53^{cKO}* SCCs (Extended Data 5d-f). Immunostaining confirmed the sustained expression of these pro-epithelial TFs (Sox2, p63, or Klf4) in *Fat1cKO* hybrid EMT cells (Figure 4j and Extended Data 5g). To identify the TFs responsible for maintaining the hybrid epithelial phenotype, we performed motif discovery analysis in the ATAC-seq peaks that were upregulated in Epcam- *Fat1cKO* TCs as compared to Epcam- control TCs from fully mesenchymal *Lgr5CREER/KRas^{G12D}/p53^{cKO}* SCCs. We found that AP1, Sox, Klf, Lhx and MafK motifs were strongly statistically enriched in Epcam- *Fat1cKO* TCs (Figure 4h, Extended Data 5d), suggesting that the epithelial program of the hybrid EMT state in *Fat1cKO* is mediated by an AP1/Sox2/Klf transcriptional network. The AP1 TF can induce chromatin remodelling in Ras driven cancers at both epithelial and mesenchymal enhancers. YAP1/Tead cooperate with AP1 to promote skin tumor initiation and EMT [35-42]. *SOX2* is amplified in many human SCCs and marks cancer stem cells in skin SCCs [43,44], and could be responsible for the hybrid EMT state and the sustained expression of epithelial genes in *Fat1cKO* TCs.

To functionally validate the bio-informatic prediction of the gene regulatory network that controls the hybrid EMT state in *Fat1* deficient tumors, we assessed the impact of CRISPR/Cas9 mediated deletion of *Yap1*/*Taz* and *Sox2* on tumor stemness, metastasis and gene expression program of mouse skin SCCs. Limiting dilution transplantation of *Sox2* KO and *Yap1/Taz* KO primary Epcam negative cell lines derived from *Lgr5CREER/KRas^{G12D}/p53^{cKO}/Fat^{cKO}* SCCs displayed a decreased TPC frequency in both cases (Fig. 4k). The number of metastasis was also importantly reduced upon deletion of either *Sox2* or *Yap1/Taz* (Fig. 4l), demonstrating that Sox2 and Yap1/Taz transcriptional programs are important for the promotion of tumor stemness and metastasis downstream of *Fat1* deletion in mouse tumors. To assess the human relevance of these findings, we performed CRISPR/Cas9 deletion of either *SOX2* or *YAP1/TAZ* in *FAT1* deleted human SCC cell lines. *SOX2* or *YAP1/TAZ* KO decreased the promotion of tumor growth mediated by *FAT1* deletion in 3D spheroid assays (Fig. 4m), demonstrating that SOX2 and YAP1/TAZ promote tumor growth downstream of *FAT1* in human cancer cells. Conversely, the deletion of *E-cadherin/ CDH1* in the same cell line, which induced defects of cell adhesion and a moderate increase in tumor growth, did not induce SOX2 or ZEB1 expression, or increase in nuclear YAP1 (Extended Data 6a-c). Conversely the overexpression of *E-cadherin/ CDH1* in *FAT1* KO cells did not decrease the clonogenicity or the expression of mesenchymal genes induced by *FAT1* deletion (Extended Data 6d-f), showing that the promotion of tumor stemness or hydrid EMT phenotype by *FAT1* deletion is not simply the results of a defect in cell adhesion.

To assess the respective role of *Sox2* and *Yap1/Taz* in the transcriptional program mediated by *Fat1* deletion, we assessed the FACS profile, histology, expression of epithelial and mesenchymal markers and transcriptional profile in *Fat1* mutated tumors presenting simultaneous deletion of *Sox2* or *Yap1/Taz* following their transplantation into

immunodeficient mice. Deletion of *Sox2* in *Lgr5CREER/KRas^{G12D}/p53^{cKO}/Fat^{cKO}* SCCs resulted in the loss of epithelial characteristics and a shift from hybrid to complete EMT, as shown by immunostaining (complete loss of Krt14) and FACS analysis (shift from hybrid to late EMT TP subpopulation) (Fig. 4n-q). The RNA-seq of *Fat1*/*Sox2* double KO further demonstrated a significant enrichment in late EMT signature (Fig. 4r), marked by an increase of mesenchymal markers (e.g. Lox, Col4a6, Mmp9, Pdgfra) and a decrease of epithelial markers (e.g. Cebpa, Krt5, Trp63) (Fig. 4s and data not shown).

Instead, the deletion of *Yap/Taz* promoted early hybrid EMT state as shown by an enrichment of Epcam- Triple Negative (TN) population and an absence of TCs presenting late EMT stages (Fig. 4t,u). The transcriptome of *Fat1/Yap1/Taz* triple KO showed significant enrichment of Epcam+ epithelial and early hybrid EMT (TN) signature (Fig. 4v). Among the genes downregulated in *Fat1/Yap1/Taz* triple KO, we found that many classical canonical *Yap1/Taz* target genes (e.g. Ctgf, Amotl2, Fstl1) as well as many other genes associated with EMT (e.g. Vcam1, Thy1, Pdfrb), were decreased compared to *Fat1* LOF (Fig.4w). Altogether these data demonstrate that Sox2 and Yap1/Taz control distinct transcriptional programs leading to a stable hybrid EMT phenotype downstream of *Fat1* LOF.

Phosphoproteomic analysis identifies the signaling cascades downstream of *FAT1* deletion

To understand how the deletion of *Fat1*, a protocadherin which is located at the plasma membrane, leads to the activation of a transcriptional program controlled by *Sox2* and *Yap1/Taz*, we performed phosphoproteomic analysis of WT and CRISPR/Cas9 *FAT1* KO human SCC cells, to dissect step by step the signaling pathways that are activated downstream of *FAT1* deletion. We quantified the phosphopeptides that were differentially

regulated between WT and *FAT1* deleted isogenic human SCC cell lines. We found that 288 phosphosites were significantly upregulated and 335 were significantly downregulated in *FAT1* KO TCs as compared to *FAT1* WT (Fig. 5a).

Upon *FAT1* LOF we observed massive decrease in the phosphorylation of the proteins involved in cell-cell adhesion, such as ZO-1 (S1617) and ZO-2 (S130, S131, S1159, S986, S226). MAP4K4, that has been reported to phosphorylate LATS1, inhibiting YAP1 and decreasing YAP1-TEAD4 interaction [45], was among the most strongly upregulated kinases in *FAT1* WT TCs (Fig. 5b). In addition, we identified PRKCD (S304) EGFR (T693), ERBB2 (S998), MEK1 (T386), MEK2 (S226), AKT2 (phosphorylated on T451), and MTOR (T1162) among the proteins that were significantly more phosphorylated in *FAT1* WT TCs (Fig. 5b, Extended Data 7a,b). In good accordance with the phosphoproteomic analysis and validating our prediction about the pathways downregulated upon *FAT1* LOF, MEK was significantly more phosphorylated and the total levels of EGFR and pEGFR were increased in *FAT1* WT TCs (Fig. 5c,d). These data suggest that the activity of the EGFR-RAS-RAF-MEK-MAPK and of the EGFR-PI3K-AKT-MTOR signaling pathways is decreased upon *FAT1* LOF.

Conversely, FAT1-deficient TCs exhibited a strong increase in the phosphorylation on Y194 of the proto-oncogene tyrosine-protein kinase YES that belongs to the SRC Family of Tyrosine Kinases (Fig. 5e, Extended Data 7c), as well as of the MAP1B (S1252, S1779, T948, T948, S2098, S937, S1298 and S1312) and GJA1 (S306, S328, S325, S330, T326, S365 and S364) proteins. GJA1 phosphorylation promotes the localization of GJA1 at the membrane and increases functional gap junction formation, which has been linked to increased metastatic capacity of TCs [46-48]. These data suggest that *FAT1* LOF induces a global remodelling of cell-cell adhesions, intercellular communications and cellular cytoskeleton leading to acquisition of hybrid EMT phenotypes.

To decipher the signaling cascade acting downstream of *FAT1* LOF, we used PhosphoSitePlus online tool [49] and bibliographic search to predict kinases acting upstream of identified phosphosites. Interestingly, Ca2+/Calmodulin-dependent protein kinase II (CAMK2) was most frequently found to act upstream of phosphopeptides enriched in *FAT1* KO TCs (CAMK2 was predicted to phosphorylate CD44 on Serine 706 [50] and GJA1 on S328, S325, S306, S330, S364 and S365) [51] (Fig. 5f, Extended Data 7d). PLK1 was another kinase frequently found to be upstream of phosphopeptides enriched upon *FAT1* LOF (Extended Data 7d).

We then used western blot (WB) to validate these findings and used small molecule inhibitors of the different kinases to define the functional relevance of the predicted kinase-protein networks. According to the bio-informatic prediction we found that CAMK2 is significantly more phosphorylated upon *FAT1* LOF (Fig. 5g). We further confirmed that SRC/YES was also more expressed and phosphorylated upon *FAT1* LOF (Fig. 5h) and that CAMK2 inhibitor (KN93) greatly decreased SRC/YES phosphorylation levels (Fig. 5i), showing that CAMK2 directly or indirectly phosphorylates YES/SRC upon *FAT1* LOF.

CD44 is a protein previously reported to be upregulated during EMT, and to promote tumor stemness, tumor progression and metastasis [27,52]. Computational analysis predicted an ESRP1-CD44-ZEB1 loop to stabilize hybrid EMT state in human lung cancer cells [53]. Phosphorylation regulates CD44 cellular localization and signaling [54]. We found that phosphorylation on S706 was upregulated upon *FAT1* LOF (Fig. 5f). FACS analysis revealed that *FAT1* KO cells expressed higher levels of surface CD44 (Fig. 5j). To understand whether CAMK2 is responsible for the stabilization of CD44 on the membrane, we treated *FAT1* KO cells with CAMK2 inhibitor and observed that the levels of surface CD44 decreased significantly upon CAMK2 inhibition in *FAT1* KO cells (Fig. 5k,l). Importantly, CD44 signaling has been shown to promote the phosphorylation of SRC [55-57]. To determine whether

CAMK2 phosphorylates YES/SRC directly or through CD44 signaling in *FAT1* KO cells, we performed CRISPR/Cas9 *CD44* deletion in *FAT1* KO cells and found that pSRC was decreased upon *CD44/FAT1* double KO (Fig. 5m). These data demonstrate that upon *FAT1* LOF, CAMK2 activates SRC at least partially though CD44. The clonogenicity of *FAT1/CD44* KO human SCC cells decreased significantly in 3D tumor spheroid assays (Fig. 5n), demonstrating that CD44 stabilization contributes to the increase in tumor stemness observed upon *FAT1* LOF.

Then we assessed whether the hybrid EMT phenotype could be explained, at least in part, by CAMK2-SRC signaling. For that purpose, we analyzed the expression of YAP1, ZEB1, E-Cadherin and SOX2 in *FAT1* KO, *FAT1/CD44* KO cells and *FAT1* KO cells treated with CAMK2 or SRC-inhibitors. We found that *FAT1/CD44* KO tumor cells, *FAT1* KO cells treated with CAMK-inhibitor (KN93) and *FAT1* KO cells treated with SRC-inhibitor (Saracatinib or Dasatinib) presented a strong decrease in nuclear YAP1 and ZEB1, an increase in E-Cadherin expression, and were growing in more compact epithelial colonies (Fig. 5o). These results demonstrated that *FAT1* LOF activates a CAMK2/CD44/SRC/YAP/ZEB1 axis that promotes the expression of a mesenchymal program. We observed a decrease in SOX2 expression in *FAT1* KO TCs treated with CAMK2 inhibitor. However, no change in SOX2 was observed upon inhibition of the CD44/SRC cascade (Fig. 5o).

Our phospho-proteomic analysis revealed that EZH2 was significantly more phosphorylated on Thr487 in *FAT1* KO cells as compared to *FAT1* WT cells. This phosphorylation site has been reported to inactivate EZH2 [58]. EZH2 is a key part of the PRC2 complex that methylates H3 at Lys 27, mediating transcriptional repression[59]. We have previously found that this histone mark is remodeled at the *Sox2* locus during SCC formation [43]. We hypothesized that EZH2 inhibition in *FAT1* KO cells could decrease H3K27me3

repressive histone marks and thus promote the expression of *SOX2*. The global level of H3K27me3 was significantly decreased in *FAT1* KO cells (Fig. 5p), supporting the notion that EZH2 could be less active upon *FAT1* LOF. When *FAT1* KO cells were treated with CAMK2 inhibitor, the global levels of H3K27me3 increased (Fig. 5q), consistently with the notion that CAMK2 activation inhibits EZH2/PRC2 activity in TCs. To functionally assess whether EZH2 inhibition leads to a decrease in H3K27me3 marks and increased *SOX2* mRNA expression, we treated *FAT1* WT cells with an EZH2 inhibitor (GSK343). H3K27me3 was decreased and SOX2 mRNA and protein expression were increased 7 days following EZH2 inhibitor treatment in *FAT1* WT cells (Fig 5r-t), further suggesting that SOX2 is epigenetically regulated by a FAT1/CAMK2/EZH2 dependent mechanism. To further demonstrate that *FAT1* deletion decreases the repressive histone marks at the *SOX2* locus, we assessed the deposition of the H3K27me3 repressive mark in the *SOX2* promoter region in the presence or absence of FAT1. ChIP-qPCR showed that H3K27me3 marks around the *SOX2* promoter were significantly reduced upon *FAT1* deletion, supporting the notion that *FAT1* deletion regulates the expression of SOX2 through an epigenetic mechanism (Fig. 5u).

As YAP/TAZ signaling has been shown to be regulated by the stiffness of the extracellular matrix [60], we assessed whether changes in stiffness of the matrix could be responsible, at least in part, for YAP1 nuclear localization or SOX2 expression upon *FAT1* LOF. To this end, we cultured *FAT1* WT and *FAT1* KO on coverslips coated with different stiffness conditions (3 and 40 kPa) and on glass. As expected, *FAT1* WT cells presented very low nuclear YAP1 when cultured on low stiffness substrate (3KP) and high nuclear YAP1 when cultured on high stiffness substrate (40KP) or glass. Interestingly, *FAT1* KO tumor cells exhibited high levels of total and nuclear YAP1 expression even on soft substrate. Higher stiffness further increased YAP1 nuclear localization (Extended Data 8a-c). These

data demonstrate that *FAT1* loss of function constitutively activates signaling pathways leading to high YAP1 expression, causing the *FAT1* KO cells to behave in respect to YAP1 nuclear expression as if tumor cells were exposed to stiff substrate. *FAT1* WT cells were negative for SOX2 independently of the stiffness of the substrate, while *FAT1* KO cells expressed high levels of SOX2 in all conditions (Extended Data 8d), demonstrating that SOX2 is constitutively activated upon *FAT1* LOF independently of the extracellular stiffness.

Drug resistance and vulnerabilities in *FAT1* mutated tumors

The treatment of advanced SCCs from different organs, such as head and neck, oesophagus or lung, remains challenging, and the prognosis is particularly poor in metastatic disease. *FAT1* is among the most frequently mutated genes in SCCs [8-10]. To which extent *FAT1* mutations impact the response to therapy in these cancers is currently unknown. We decided to test whether the signaling cascades changed upon *FAT1* LOF could predict therapeutic resistance and vulnerability of these cancers. To test this hypothesis, we assessed the sensitivity of WT and isogenic *FAT1* KO human cancer cell lines to the inhibitors of the signaling pathways that were found to be differentially regulated between WT and *FAT1* KO cells. EGFR inhibitors such as Afatinib are widely used in patients with metastatic SCC [61,62]. MEK inhibitors also have been proposed to be an attractive therapeutic strategy in metastatic SCC [63]. Very interestingly, *FAT1* KO cells were significantly more resistant to the EGFR-inhibitor Afatinib and the MEK-inhibitor Trametinib as compared to *FAT1* WT SCC cells (Fig. 5v,x).

In sharp contrast, *FAT1* KO TCs were significantly more sensitive to the SRC inhibitors Dasatinib and Saracatinib and the CAMK2 inhibitor KN93 as compared to *FAT1* WT TCs (Fig. 5w,x). These results suggest that our understanding of the molecular

mechanisms underlying *FAT1* LOF can lead to a much better targeted therapy in patients with *FAT1*-mutated cancers.

Discussion.

Our study reveals that *Fat1* deletion, one of the most frequently mutated tumor suppressor genes[1-9], promotes the acquisition of a hybrid EMT state presenting increased tumor stemness and metastasis. We identify the epigenetic and transcriptional mechanisms that link loss of cell polarity and cell adhesion with the induction of a hybrid EMT phenotype downstream of *Fat1* deletion. Our comprehensive molecular characterization including transcriptomic, epigenomic, and proteomic characterization of *Fat1* mutants shows that the hybrid EMT signature is mediated by the activation of YAP1 and Sox2, which regulate respectively the co-expression of mesenchymal and epithelial transcriptional programs in cancer cells. Importantly, we show that the gene signature associated with *Fat1* loss of function is predictive of poor survival in lung cancer patients.

Using phosphoproteomic analysis coupled with a functional characterization of the protein phosphorylation network that is activated or inhibited upon *FAT1* deletion, we identified the signaling cascades leading to the activation of YAP1 and SOX2 downstream of *FAT1* LOF. *FAT1* deletion activates CAMK2, which induces the phosphorylation of SRC/YES and CD44, which promote YAP nuclear translocation and the induction of an EMT program including ZEB1 expression. CAMK2 activation also leads to the phosphorylation of EZH2 at Thr487, which inhibits its activity [58] and causes a decrease of the chromatin repressive mark H3K27me3 at *SOX2* regulatory regions, which leads to SOX2 upregulation, sustaining the expression of the epithelial program. In addition, *FAT1* deletion also decreases the activation of the EGFR/MEK pathway. Very interestingly, the activation and inhibition of these signaling pathways lead to an increased sensitivity of *FAT1* mutated

cancer cells to CAMK2 and SRC inhibition and to resistance to EGFR and MEK inhibition (Extended Data 8e). This study has important implications for personalized medicine and the prognosis and treatment of the high number of patients with cancer displaying *FAT1* mutations.

ACKNOWLEDGMENTS

We thank ULB animal facility and ULB genomic core facility (Frederick Libert and Anne Lefort). We thank Justine Allard from CMMI for her help to perform IHC in human PDX. I.P. is supported by FNRS. The Department of Pathology acknowledges Fonds Yvonne Boel. C.Dec. is a senior research associate in F.R.S.-FNRS. The CMMI is supported by the European Regional Development Fund and the Walloon Region. PDX platform is supported by Fonds Erasme. C.Bla is supported by WELBIO, FNRS, Fond Erasme, Fondation Contre le Cancer, ULB Foundation, European Research Council, Worldwide Cancer Research and the Foundation Baillet Latour.

AUTHOR CONTRIBUTION

I.P., F.M. and C.Bla designed the experiments and performed data analysis. I.P. and F.M. performed most of biological experiments. F.H. generated *Fat1cKO* mice and provided her expertise. F.dC helped to perform CRISPR experiments. B. M. performed intratracheal AdenoCRE instillation for lung cancer generation. F.I and D.V.H. performed phosphoproteomic analysis. M.O and M.T. performed stiffness experiments. M.V. and D.P-M performed EM imaging and analysis. Y.B. and C.S. performed analysis of patient survival using TCGA database. I.S., Y.S., S.H., B.A.M., L.R.B., P.J., P.R, R.S.G, N.d.H and I.S. provided human samples. C.Bal and C.Dec performed staining and analysis of PDX samples. C.Dub performed FACS sorting. V.M, S.L, G.L., J.B., M.R. and S.S performed immunostainings, WB, treatments and follow-up of the mice. All authors read and approved the final manuscript.

AUTHOR INFORMATION

No competing financial interests.

FIGURE LEGENDS

Figure 1. *Fat1* loss of function accelerates DMBA/TPA tumor initiation and malignant progression. a, Mouse model allowing constitutive *Fat1* deletion in the skin epidermis and the scheme of DMBA/TPA induced skin SCCs. **b**, Image showing control and *Fat1cKO* littermates 24 weeks after initiation of DMBA/TPA treatment. **c**, Graph showing the time from the beginning of DMBA/TPA treatment until the appearance of the first tumor in control and *Fat1cKO* mice. Log-rank Mantel-Cox test. **d**, Number of papillomas in control and *Fat1cKO* mice 32 weeks after DMBA/TPA treatment. Mean±SEM, two-tailed T-test **e**, Images showing the macroscopic appearance of papilloma and carcinoma in DMBA/TPA induced skin tumors. **f**, Number of carcinomas per mouse at 32 weeks after DMBA/TPA in control and *Fat1KO* mice. Mean±SEM, two-tailed T-test. **g**, Acute deletion of *Fat1* in DMBA/TPA induced papillomas. **h**, Kaplan Meier plot showing the time from Tamoxifen (Tam) administration to macroscopic malignant progression from papillomas into carcinomas. Log-rank Mantel-Cox test. **i**, Graph showing the proportion of papillomas that progressed to carcinomas in control and *Fat1cKO* mice after Tam administration. **j, k** Immunostaining for Krt14, Krt10 and Lam5 in control (j) and *Fat1cKO* papillomas (k) 0, 2, 4 and 8 weeks after Tam administration (n=12 mice, n=24 control papillomas and n=10 mice, n=20 *Fat1cKO* papillomas). Scale bar=50μm. **l**, Hematoxilin-Eosin and immunostaining for YFP, E-Cadherin, Zo-1 or Cldn1 in Control and *Fat1cKO* papillomas. Scale bar Scale bar=50μm. **m**, Electron microscopy (EM) images showing columnar basal cells oriented perpendicularly to the basal lamina in control papillomas and loss of polarity and adhesion in basal layer of *Fat1cKO* papillomas. Red lines indicate interface between tumor cells (TCs) and stroma. Scale bar control papilloma=2μm, Scale bar *Fat1cKO* papilloma=5μm. **n**, EM images showing intercellular junctions. Blue arrowheads indicate desmosomes. Red

arrowheads indicate tight and adherens junctions in control papilloma that are lost in *Fat1cKO* papilloma. Scale bar=0.2 μm. **o**, EM image showing at higher magnification the desmosomes in control and *Fat1cKO* papillomas. Blue arrowheads indicate desmosomes. Scale bar=0.2 μm. **p**, Graph showing the width of the desmosomes measured in nm in control and *Fat1cKO* papillomas. Mean±SEM, two-tailed T-test. **q**, EM (Control papilloma Scale bar=0.2μm; *Fat1cKO* papilloma Scale bar=0.5μm) and immunostaining for Krt14 and Lam5 (Scale bar=50μm) of control and *Fat1cKO* papillomas. Blue arrowheads indicate hemidesmosomes. Red arrowheads indicate basal lamina in control papillomas and discontinued basal lamina in *Fat1cKO* papillomas. Black arrowheads show fenestration of basal lamina in *Fat1cKO* papillomas. **r**, Number of hemidesmosomes per 1μm (n=32 desmosomes, n=2 papillomas, n=2 mice in control mice; n=19 desmosomes, n=2 papillomas n=2 mice in *Fat1cKO* mice). Mean±SEM, two-tailed T-test.

Figure 2. *Fat1* loss of function promotes hybrid EMT state in mouse skin SCC, mouse lung cancer and human SCC. **a**, Immunostaining for GFP, E-cadherin, Vimentin, Krt14 and Vimentin in Epcam+ Control, Epcam+ *Fat1cKO* and Epcam- *Fat1cKO* DMBA/TPA carcinomas. Scale bar=50μm. **b**, FACS histograms showing Epcam expression in representative control and *Fat1cKO* YFP+ skin SCC TCs. **c**, Percentage of Epcam+ YFP+ TCs in control and *Fat1cKO* DMBA/TPA carcinomas. Mean±SEM, two-tailed T-test. **d**, Distribution of YFP+ Epcam- TC subpopulations based on CD106/Vcam1, CD61/Itgb3 and CD51/Itgav expression in *Fat1cKO* skin SCCs. Mean±SEM **e**, Co-immunostaining for Krt14 and Vimentin in cytospin of FACS-isolated YFP+Epcam+ Control, YFP+Epcam+ and Epcam- *Fat1cKO* TCs. Scale bar=20μm. **f**, Quantification of Krt14 and Vimentin expression in cytospin of skin SCC TCs (n=90 cells per condition and tumor). **g**, Immunostaining for GFP, Krt7, Nkx2-1, Krt5, Sox2, Krt8/18 and Vimentin in Epcam+ Control, Epcam+ and

Epcam- *Fat1cKO* lung carcinomas. Scale bar=50µm. **h**, FACS histograms showing Epcam expression in representative control and *Fat1cKO* YFP+ lung TCs. **i**, Percentage of Epcam+ YFP+ TCs in control and *Fat1cKO* lung carcinomas. Mean±SEM, two-tailed T-test. **j**, Distribution of YFP+ Epcam- TC subpopulations based on CD106/Vcam1, CD61/Itgb3 and CD51/Itgav expression in *Fat1cKO* lung carcinomas. Mean±SEM. **k**, Co-immunostaining for Pancytokeratin and Vimentin in cytospin of FACS-isolated YFP+Epcam+ Control, YFP+Epcam+ and Epcam- *Fat1cKO* lung carcinoma TCs. Scale bar=20µm. **l**, Quantification of Pancytokeratin and Vimentin expression in cytospin of lung carcinoma TCs (min. n=70 cells per condition and tumor). **m**, Immunostaining for Krt14, Vim, E-Cadherin, Claudin-1, Sox2, p63 and Zeb1 in *FAT1* WT and CRISPR/Cas9 *FAT1 KO* A388 human skin SCC cell line. Scale bar=50µm. **n,** Representative images of computer-assisted reconstruction of co-localization of Pan-cytokeratin and Vimentin in *FAT1* wild type (WT) and *FAT1* mutated Head and Neck and Lung Patient Derived Xenografts (PDX). Scale bar=50µm. **o**, Plot showing hybrid EMT score in *FAT1* WT and *FAT1* PDX (defined as number of double positive pan-cytokeratin/vimentin TCs divided by total number of Ku-80+ human TCs). Mean±SEM, two-tailed Mann-Whitney U test.

Figure 3. *Fat1* deletion promotes tumor stemness and metastasis in skin SCCs.

a, Schematic showing the strategy to estimate tumor propagating cell (TPC) frequency and table showing frequency of secondary tumors observed upon subcutaneous transplantation of limiting dilutions of YFP+ Epcam+ Control tumor cells, YFP+ Epcam+ and total YFP+ *Fat1cKO* tumor cells and the estimation of the TPC using Extreme Limiting Dilution analysis (ELDA) (Chi-square test). **b**, Immunostaining for GFP, Krt14 and Vimentin in the secondary

tumors arising after subcutaneous transplantation of TCs. Scale bar=50μm. **c**, Images showing spheroids formed 7 days after plating 4000 *FAT1* WT or *FAT1* KO human A388 skin SCC cells in ultra-low attachment plate. **d**, Bar chart showing the quantification of cell number in *FAT1* WT and *FAT1* KO spheroids (Mean±SEM, two-tailed T-test). **e**, Plot showing the proportion of mice presenting lymph node (LN) metastasis (mean percentage, two-tailed T-test). **f**, Dot plot showing the number of LN metastasis per mouse (Mean±SEM, two-tailed T-test). **g**, Plot showing the proportion of mice presenting lung metastasis (mean percentage, two-tailed T-test). **h**, Dot plot showing the number of lung metastasis per mouse (Mean±SEM, two-tailed T-test). **i**, Schematic drawing showing the strategy to assess lung extravasation of Epcam+ TCs following intravenous injection. **j**, Plot showing the proportion of mice presenting lung metastasis 40 days after intravenous injection of 20.000 YFP+ TCs (mean percentage, two-tailed T-test). **k**, Mosaic images of immunostaining for YFP of lungs after intravenous injection of control or *Fat1cKO* tumor cells. **l**, Dot plots showing the number of metastases per lung arising from the injection of 20.000 YFP+ Epcam+ *Fat1* WT and YFP+ Epcam+ *Fat1cKO* TCs (Mean±SEM, two-tailed T-test).

Figure 4. Yap1 and Sox2 regulate mesenchymal and epithelial states downstream of *Fat1* deletion.

a, mRNA expression of mesenchymal genes defined by RNA-seq in Epcam+ and Epcam- *Fat1* WT and *Fat1cKO* skin SCC cells (mean+SEM). **b**, mRNA expression of epithelial genes defined by RNA-sequencing in Epcam+ and Epcam- *Fat1* WT and *Fat1cKO* skin SCC cells (mean+SEM). **c**, Venn diagram of the genes upregulated in the Epcam+ *Fat1cKO* skin SCC TCs and naturally upregulated genes in Epcam+ as compared to the hybrid EMT triple negative (TN) TCs (Two-sided hypergeometric test). **d**, Venn diagram of the genes upregulated in the Epcam+ *Fat1cKO* skin SCC TCs and naturally upregulated genes in TN as

compared to Epcam+ TCs (Two-sided hypergeometric test). **e**, mRNA expression of mesenchymal genes defined by RNA-seq in Epcam+ *Fat1* WT and Epcam+ and Epcam- *Fat1cKO* lung carcinoma cells (n=2, mean+SEM). **f**, mRNA expression of mesenchymal genes defined by RNA-seq in *FAT1* WT and *FAT1* KO human SCC cells (n=2, mean+SEM). **g,** Graph showing the overall survival of patients with lung squamous cell carcinoma (SCC) stratified by the expression of genes commonly upregulated in mouse skin and lung *Fat1cKO* SCC cells and in human skin SCC *FAT1* KO TCs (Long Rank Mantel Cox test) **h**, TF motifs enriched in the ATAC-seq peaks up-regulated between the Epcam+ *Fat1cKO* and Epcam+ *Fat1* WT and between Epcam- *Fat1cKO* and Epcam- *Fat1* WT skin SCC TCs as determined by Homer. **i**, Immunohistochemistry showing YAP1 expression in *Fat1* WT and *Fat1cKO* skin SCCs. Scale bar=50µm. **j**, Immunostaining for GFP and Sox2 in *Fat1* WT and *Fat1cKO* DMBA/TPA and *Lgr5CREER/KRas^{G12D}/p53^{cKO}* skin SCCs. Scale bar=50µm. **k**, Table showing frequency of secondary tumors observed upon subcutaneous transplantation of limiting dilution of YFP+ Epcam- *Fat1* KO, YFP+ Epcam- *Fat1/Sox2* KO and YFP+ Epcam- *Fat1/Yap1/Taz* KO skin SCC TCs and the estimation of the TPC using Extreme Limiting Dilution analysis (ELDA) (Chi-square test). **l**, Graph showing the number of lung metastasis arising from the injection of 1000 YFP+ Epcam- *Fat1* KO, YFP+ Epcam- *Fat1/Sox2* KO and YFP+ Epcam- *Fat1/Yap1/Taz* KO skin SCC TCs (Mean±SEM, two-tailed T-test). **m**, Bar chart showing the number of cells in spheroids formed by *FAT1* KO, *FAT1/YAP1/TAZ* KO and *FAT1/SOX2* KO human SCC cells 7 days after plating 4000c in ultra-low attachment plate (Mean±SEM, two-tailed T-test). **n**, Distribution of YFP+ Epcam- TC subpopulations based on CD106/Vcam1, CD61/Itgb3 and CD51/Itgav expression in *Fat1cKO* mouse skin SCC-derived cell lines after subcutaneous transplantation (n=5). **o**, Immunostaining for GFP, Krt14 and Vim in representative SCC arising from subcutaneous transplantation of *Fat1cKO* skin SCC-derived cell lines. Scale bar=50µm. **p**, Distribution of YFP+ Epcam- TC

subpopulations based on CD106/Vcam1, CD61/Itgb3 and CD51/Itgav expression in *Fat1/Sox2* KO mouse skin SCC cell lines after subcutaneous transplantation (n=6). **q**, Immunostaining for GFP, Krt14 and Vim in representative SCC arising from subcutaneous transplantation of *Fat1/Sox2* KO SCC cell lines. Scale bar=50μm. **r**, Venn diagram of the genes upregulated in Epcam- *Fat1cKO* skin SCC TCs upon *Sox2* deletion and naturally upregulated genes in hybrid EMT triple negative (TN) (CD106-/CD51-/CD61-) TCs as compared to late EMT triple positive (TP) CD106+/CD51+/CD61+) tumor cells (early hybrid EMT signature) and in TP as comparted to Epcam+ TCs (late EMT signature) (Two-sided hypergeometric test). **s**, mRNA expression of epithelial genes and genes associated with polarity controlled by *Sox2* defined by RNA-seq in Epcam- *Fat1cKO* and *Fat1/Sox2* KO skin SCC cells (Mean+SEM). **t**, Distribution of YFP+ Epcam- TC subpopulations based on CD106/Vcam1, CD61/Itgb3 and CD51/Itgav expression in *Fat1/Yap1/Taz1* KO mouse skin SCC cell lines after subcutaneous transplantation (n=5). **u**, Immunostaining for GFP, Krt14 and Vim in representative SCC arising from subcutaneous transplantation of *Fat1/Yap1/Taz1* KO SCC cell lines. Scale bar=50μm. **v**, Venn diagram of the genes upregulated in Epcam- *Fat1cKO* skin SCC TCs upon *Yap1/Taz* deletion and naturally upregulated genes in hybrid EMT triple negative (TN) TCs as compared to late EMT Triple Positive (TP) TCs (early hybrid EMT signature) and in TP as comparted to Epcam+ TCs (late EMT signature) (Two-sided hypergeometric test). **w**, mRNA expression of Yap1/Taz target genes and other mesenchymal genes regulated by Yap1/Taz defined by RNA-seq in Epcam- *Fat1cKO* and *Fat1/Yap1/Taz* KO skin SCC cells (mean+SEM) (n=2).

Figure 5. Phosphoproteomic analysis identifies the signaling cascades downstream of *FAT1* deletion. a, Volcano plot showing the Fold Change (in $\log_2$ on the X-axis) of each phosphopeptide between *FAT1* WT and *FAT1* KO sample and statistical significance (-Log p

value on the Y-axis) (t-test, FDR=0.05 and S_0=1). **b**, Table showing the phosphorylation sites of the different kinases significantly upregulated in *FAT1* WT as compared to *FAT1* KO. **c**, Western Blot showing the expression levels of phosphorylated MEK1/2 (antibody recognizes phosphorylation of MEK 1/2 on Ser218, SER222, Ser226) and total MEK in *FAT1* WT and *FAT1* KO cells. **d**, Western Blot showing the expression levels of phosphorylated EGFR (antibody recognizes phosphorylation of EGFR on Y1197) and total EGFR in *FAT1* WT and *FAT1* KO cells. **e**, Table showing the enrichment of YES1 Y194 phosphosite in *FAT1* KO vs WT. **f**, Table showing the phosphosites predicted to be phosphorylated by CAMK2 enriched in *FAT1* KO cells **g**, Western Blot showing the expression levels of phosphorylated CAMK2 (antibody recognizes phosphorylation of CAMK2alpha on Thr286, and CAMK2beta and gamma on Thr287) and total CAMK2 proteins in *FAT1* WT and *FAT1* KO cells. **h**, Western Blot showing the expression levels of phosphorylated SRC (antibody recognizes phosphorylation of YES/SRC on Tyr416), total SRC and YES proteins in *FAT1* WT and *FAT1* KO cells. **i**, Western Blot showing the expression levels of phosphorylated SRC, total SRC and YES proteins in *FAT1* KO cells treated with DMSO or with CAMK2 inhibitor (KN93). **j**, Histograms showing the expression of CD44 by FACS in *FAT1* WT and *FAT1* KO TCs. **k**, Histograms showing the expression of CD44 by FACS in *FAT1* KO TCs treated with DMSO or with 10uM CAMK2 inhibitor (KN93) (n=16). **l**, Bar chart showing the proportion of *FAT1* KO TCs expressing high levels of CD44 treated with DMSO or with CAMK2 inhibitor (Mean+SEM, two-tailed T-test). **m**, Western Blot showing the expression levels of phosphorylated SRC, total SRC and YES proteins in *FAT1* KO and *FAT1/CD44* KO TCs. **n**, Bar chart showing the quantification by FACS of the number of cells in *FAT1* WT and *FAT1/CD44* KO spheroids (Mean+SEM, two-tailed T-test). **o**, Immunostaining for E-cadherin, CD44, YAP1, ZEB1 and SOX2 in *FAT1* KO cells treated with DMSO, with SRC inhibitor (Saracatinib), CAMK2 inhibitor (KN93) and *FAT1/CD44* KO TCs. Scale

bar=50µm. **p**, Western blot showing the expression levels of H3K27me3 mark and H3 proteins in *FAT1* WT and *FAT1* KO cells. **q**, Western Blot showing the expression levels of H3K27me3 mark and H3 proteins in *FAT1* KO TCs treated with DMSO or with CAMK2 inhibitor (KN93). **r,** Western Blot showing the expression levels of H3K27me3 mark and H3 proteins in *FAT1* WT cells treated with DMSO or with EZH2 inhibitor (GSK343). **s,** Dot plot showing *SOX2* mRNA expression by RT-qPCR in *FAT1* WT cells treated during 7 days with DMSO or with EZH2-inhibitor (GSK343) (Mean±SEM, two-tailed T-test). **t**, Western Blot showing the expression level of SOX2 protein in *FAT1* WT cells treated during 7 days with DMSO or with EZH2-inhibitor (GSK343). **u**, ChIP-qPCR showing different levels of H3K27me3 mark deposition in the genomic region surrounding *SOX2* TSS in *FAT1* WT and KO cells. The data represent the ratio of relative enrichment of the indicated genomic regions in *Fat1* WT vs KO cells. Ctrl1 and 2 are negative control regions for EZH2/H3K27me3. (One sample T-test, Mean±SEM. Control 1 n=3, p=0.61; Control 2 n=3, p=0.63; -0.5 n=3, p=0.04; 0.1 n=3, p=0.008; 0.5 n=3, p=0.006; 0,7 n=3, p=0.02). **v**, Representative dose-response curve showing the effect of increasing doses of EGFR-inhibitor Afatinib on *FAT1* WT and *FAT1* KO cell viability at 48h analysed by FACS (normalized to the average of 5 wells treated with DMSO). Non-linear regression log(inhibitor) with least squares fit method (n=3, Mean±SEM). **w,** Representative dose-response curve showing the effect of increasing doses of SRC-inhibitor Dasatinib on *FAT1* WT and *FAT1* KO cell viability at 48 hours analysed by FACS (normalized to the average of 4 wells treated with DMSO). Non-linear regression log(inhibitor) with least squares fit method (n=3, Mean±SEM). **x**, Table showing the summary (n=3) of pIC50 and SEM for different drugs for *FAT1* WT and *FAT1* KO cells (two-tailed T-test).

EXTENDED DATA FIGURE LEGENDS

Extended Data 1. *Fat1* loss of function does not alter development and skin homeostasis. **a**, Image showing *Fat1cKO* mouse and its control littermate. **b,** Table showing the number of control mice and mice with constitutive *Fat1cKO* in skin epidermis, showing the absence of deviation from Mendelian ratio. **c,** Hematoxilin-Eosin staining in control and *Fat1cKO* epidermis. Scale bar=50µm. **d**, **e**, Immunostaining for GFP and Krt10, Krt14, E-Cadherin or Itgb4 in control (d) and *Fat1cKO* (e) epidermis. Scale bar=50µm. **f,** Percentage of Epcam+ YFP+ TCs in control and *Fat1cKO* DMBA/TPA papillomas (n=3, Mean±SEM, two-tailed T-test). **g**, mRNA expression of selected epithelial genes as defined by RT-qPCR in Epcam- *Fat1* WT and *Fat1cKO* papilloma cells (n=3, Mean+SEM). **h**, mRNA expression of selected mesenchymal genes as defined by RT-qPCR in Epcam- *Fat1* WT and *Fat1cKO* papilloma cells (n=3, Mean+SEM).

Extended Data 2. Gating strategy for FACS analysis and cell sorting of the different tumor subpopulations. **a**, FACS plots showing the gating strategy used to FACS isolate or to analyse the proportion of YFP+ Epcam+ and Epcam- TCs from DMBA/TPA *K14CRE/Fat1^{cKO}/Rosa26$^{YFP/+}$* carcinomas and papillomas, , *Lgr5CREER/KRas^{G12D}/p53^{cKO} /Fat1^{cKO}/Rosa26$^{YFP/+}$* or K14CREER/ *KRas^{G12D}/p53^{cKO}/Fat1^{cKO}/Rosa26$^{YFP/+}$* skin SCCs and *KRas^{G12D}/p53^{cKO} /Fat1^{cKO}/Rosa26$^{YFP/+}$* lung carcinomas. **b**, FACS plots showing the gating strategy to define the 6 different subpopulations of Epcam- TCs: Epcam-/CD106-/CD51-/CD61- (TN), Epcam-/CD106+/CD51-/CD61-, Epcam-/CD106-/CD51+/CD61-, Epcam-/CD106+/CD51+/CD61-, Epcam-/CD106-/CD51+/CD61+ and Epcam-/CD106+/CD51+/CD61+ (TP) populations.

Extended Data 3. *Fat1* loss of function promotes hybrid EMT state in genetic model of skin SCC. **a**, Mouse model of skin SCC allowing YFP and $Kras^{G12D}$ expression as well as *p53* and *Fat1* deletion preferentially in the interfollicular epidermis (IFE) using *K14CEER*. **b**, Percentage of Epcam+ TCs in control and *Fat1cKO* SCCs (n=8 control and n=7 *Fat1cKO* mice, mean±SEM, two-tailed T-test). **c**, Graph showing the distribution of the different Epcam- TC subpopulations based on the expression of CD106/Vcam1, CD61/Itgb3 and CD51/Itgav in *Fat1cKO* tumors (n=7 mice, mean±SEM). **d**, Hematoxilin-Eosin showing representative control and *Fat1cKO* tumors. Scale bar=50µm. **e**, **f** Immunostaining for GFP, Krt14 or Vimentin in representative control (e) and *Fat1cKO* tumor (f) (n=8 control tumors, n=8 mice and n=9 *Fat1cKO* tumors, n=7 mice). Scale bar=50µm. **g**, Mouse model of skin SCC allowing the expression of YFP and $Kras^{G12D}$ as well as *p53* and *Fat1* deletion preferentially in the hair follicle lineage using *Lgr5CREER*. **h**, Percentage of Epcam+ TCs in the control and *Fat1cKO* tumors (n=15 control and n=12 *Fat1cKO* mice, mean±SEM, two-tailed T-test). **i**, Graph showing the distribution of the different Epcam- TC subpopulations based on the expression of CD106/Vcam1, CD61/Itgb3 and CD51/Itgav in *Fat1cKO* tumors (n=12 mice, mean±SEM). **j**, Hematoxilin-Eosin showing a representative *Fat1* WT and *Fat1cKO* tumors. Scale bar=50µm. **k**, **l**, Immunostaining for Krt14 and Vimentin showing the absence of keratin pearls in representative Epcam- control SCC (n=15 mice) (k) and the presence of keratin pearls in representative Epcam- *Fat1cKO* SCC (n=12 mice) (l). White arrowheads indicate keratin pearls. Scale bar=100µm. **m**, Dot plot showing the number of keratin pearls quantified per field at magnification 20X (n=7 control and n=8 *Fat1cKO*, n=5 fields quantified per sample, mean±SEM, two-tailed T-test). **n**, Mouse model allowing YFP and $Kras^{G12D}$ expression as well as *p53* and *Fat1* deletion in lung epithelial cells using intratracheal instillation of Ad5CMVCre virus. **o**, Immunofluorescence image showing the

YFP+ lung tumors 10 weeks after intratracheal instillation of Ad5CMVCre in *Fat1* WT and *Fat1cKO* mice.

Extended Data 4. Mutations in *FAT1* promotes hybrid EMT state in human cancers. a, Schematic drawing representing the method to analyse the co-expression of Pan-cytokeratin and Vimentin in IHC of Patient Derived Xenografts (PDX) presenting or not mutations in *FAT1* and the definition of hybrid EMT score. **b**, Table summarizing the samples of PDX on which Whole Exome Sequencing was performed and the detailed information on the mutations: codon, AA change, the exon harbouring the mutation, the allelic frequency, the type of mutations and the bioinformatic prediction of the impact of the mutation on the function of the protein by 3 different bioinformatic algorithms (SIFT, Memo and PolyPhen) [64-66]. **c**, Heatmap showing the Copy Number Variation (CNV) profile of *FAT1* genomic region in the PDX samples included in the analysis of hybrid EMT score. The color code corresponds to the quantified copy number and the genomic coordinate (reference genome hg19) of bin set for quantification. The *FAT1* gene is marked on each vertical edge. **d**, Box Plot showing the distribution of the common mRNA signature (mouse skin and lung *Fat1cKO* SCCs and human *FAT1* KO SCC cell line) compared to *FAT1* mutation status in human Lung SCC (TCGA database) (For the analysis only high impact mutations in >20% of variant allele frequency were considered. Mean, the lowest and the highest values, Wilcox Rank Sum test). **e**, Box Plot showing the distribution of the common mRNA signature (mouse skin and lung *Fat1cKO* SCCs and human *FAT1* KO SCC cell line) compared to *FAT1* Copy Number Variation (CNV) status in human Lung SCC (TCGA database) (Mean±SD, Wilcox Rank Sum test).

Extended Data 5. Epcam+ *Fat1cKO* tumor cells are epigenetically primed to undergo EMT while Epcam- *Fat1cKO* sustain the expression of epithelial program. a, ATAC-seq profiles of the chromatin regulatory regions of mesenchymal genes closed in control Epcam+ TCs and opened in Epcam+ *Fat1cKO* TCs, showing epigenetic priming of Epcam+ *Fat1cKO* TCs to undergo EMT. **b**, ATAC-seq profiles of the chromatin regulatory regions of mesenchymal genes with open chromatin regions only in EMT Epcam- TCs. **c**, TF motifs enriched in the ATAC-seq peaks up-regulated between the Epcam+ *Fat1cKO* and Epcam+ control TCs as determined by Homer. White boxes show core TFs, boxes highlighted in green show epithelial TFs and boxes highlighted in orange show EMT TFs. **d**, TF motifs enriched in the ATAC-seq peaks up-regulated between the Epcam- *Fat1cKO* and Epcam- control TCs as determined by Homer analysis. White boxes show core TFs, boxes highlighted in green show epithelial TFs, boxes highlighted in orange show EMT TFs and boxes highlighted in grey show other TFs. **e**, ATAC-seq of the chromatin regulatory regions of epithelial genes with open chromatin regions in Epcam- *Fat1cKO* TCs as compared to Epcam- TCs from Lgr5 derived SCCs, showing the sustained opening of epithelial enhancers in Epcam- *Fat1cKO* TCs. **f**, ATAC-seq of the chromatin regulatory regions of epithelial genes that are closed upon EMT irrespective of *Fat1* deletion. **e**, Immunostaining for GFP and AP2g, Klf4, Sox2, p63, Grhl2 or Zeb1 in Epcam+ and Epcam- control and *Fat1cKO* DMBA/TPA skin SCCs. Scale bar=50μm.

Extended Data 6. **Loss of cell adhesion is not sufficient to induce hybrid EMT phenotype. a**, Images showing spheroids formed 7 days after plating 4000 *FAT1* WT or *FAT1* WT / *CDH1* KO human A388 skin SCC cells in ultra-low attachment plate. **b**, Bar chart showing the quantification by FACS of the number of cells in *FAT1* WT and *FAT1* WT / *CDH1* KO spheroids (Mean+SEM, two-tailed T-test). **c**, Immunostaining for E-cadherin,

YAP1, ZEB1 and SOX2 in *FAT1* WT and *FAT1* WT / *CDH1* KO TCs. **d**, Images showing spheroids formed 7 days after plating 4000 *FAT1* KO or *FAT1* KO / *CDH1* Overexpression (OE) human A388 skin SCC cells in ultra-low attachment plate. **e**, Bar chart showing the quantification by FACS of the number of cells in *FAT1* KO or *FAT1* KO / *CDH1* OE spheroids (Mean+SEM, two-tailed T-test). **f,** Immunostaining for E-cadherin, YAP1, ZEB1 and SOX2 in *FAT1* KO or *FAT1* KO / *CDH1* OE TCs.

Extended Data 7. Phosphoproteomic analysis reveals signaling cascades downstream of *FAT1* loss of function. a, Table showing kinases significantly more phosphorylated in *FAT1* WT cells as compared to *FAT1* KO. **b**, Bar chart showing the kinases that are predicted to phosphorylate phosphosites significantly enriched in *FAT1* WT TCs. **c,** Table showing kinases significantly more phosphorylated in *FAT1* KO cells as compared to *FAT1* WT. **d**, Bar chart showing the kinases that are predicted to phosphorylate phosphosites significantly enriched in *FAT1* KO TCs.

Extended Data 8. Increase in Yap1 and Sox2 signalling downstream of *FAT1* LOF is independent of the stiffness of the substrate.

a, Immunostaining for YAP1 in *FAT1* WT and *FAT1* KO human SCC cells upon increasing stiffness conditions. Scale bar=50μm. **b,** Quantification of YAP1 expression based on fluorescence intensity in *FAT1* WT and *FAT1* KO cells upon different stiffness conditions. **c,** Quantification of YAP1 nuclear/cytoplasmic ratio based on fluorescence intensity in *FAT1* WT and *FAT1* KO cells upon different stiffness conditions. **d,** Immunostaining for SOX2 in *FAT1* WT and *FAT1* KO human SCC cells upon increasing stiffness conditions. Scale bar=50μm **e**, Schematic showing the signaling pathways that are activated in *FAT1* WT and *FAT1* KO cells and predict a differential impact on the response to therapy.

BIBLIOGRAPHY

1 Lee, C. S. *et al.* Recurrent point mutations in the kinetochore gene KNSTRN in cutaneous squamous cell carcinoma. *Nat Genet* **46**, 1060-1062, doi:10.1038/ng.3091 (2014).

2 South, A. P. *et al.* NOTCH1 mutations occur early during cutaneous squamous cell carcinogenesis. *J Invest Dermatol* **134**, 2630-2638, doi:10.1038/jid.2014.154 (2014).

3 Pickering, C. R. *et al.* Mutational landscape of aggressive cutaneous squamous cell carcinoma. *Clin Cancer Res* **20**, 6582-6592, doi:10.1158/1078-0432.Ccr-14-1768 (2014).

4 Comprehensive genomic characterization of head and neck squamous cell carcinomas. *Nature* **517**, 576-582, doi:10.1038/nature14129 (2015).

5 Agrawal, N. *et al.* Exome sequencing of head and neck squamous cell carcinoma reveals inactivating mutations in NOTCH1. *Science* **333**, 1154-1157, doi:10.1126/science.1206923 (2011).

6 Lin, D. C. *et al.* Genomic and molecular characterization of esophageal squamous cell carcinoma. *Nat Genet* **46**, 467-473, doi:10.1038/ng.2935 (2014).

7 Mutational landscape of gingivo-buccal oral squamous cell carcinoma reveals new recurrently-mutated genes and molecular subgroups. *Nat Commun* **4**, 2873, doi:10.1038/ncomms3873 (2013).

8 Morris, L. G. *et al.* Recurrent somatic mutation of FAT1 in multiple human cancers leads to aberrant Wnt activation. *Nat Genet* **45**, 253-261, doi:10.1038/ng.2538 (2013).

9 Dotto, G. P. & Rustgi, A. K. Squamous Cell Cancers: A Unified Perspective on Biology and Genetics. *Cancer Cell* **29**, 622-637, doi:10.1016/j.ccell.2016.04.004 (2016).

10 Chen, M. *et al.* Concurrent Driver Gene Mutations as Negative Predictive Factors in Epidermal Growth Factor Receptor-Positive Non-Small Cell Lung Cancer. *EBioMedicine* **42**, 304-310, doi:10.1016/j.ebiom.2019.03.023 (2019).

11 Li, Z. *et al.* Loss of the FAT1 Tumor Suppressor Promotes Resistance to CDK4/6 Inhibitors via the Hippo Pathway. *Cancer Cell* **34**, 893-905.e898, doi:10.1016/j.ccell.2018.11.006 (2018).

12 Lin, S. C. *et al.* FAT1 somatic mutations in head and neck carcinoma are associated with tumor progression and survival. *Carcinogenesis* **39**, 1320-1330, doi:10.1093/carcin/bgy107 (2018).

13 Wang, L. *et al.* Loss of FAT1 during the progression from DCIS to IDC and predict poor clinical outcome in breast cancer. *Exp Mol Pathol* **100**, 177-183, doi:10.1016/j.yexmp.2015.12.012 (2016).

14 Yu, J. & Li, H. The expression of FAT1 is associated with overall survival in children with medulloblastoma. *Tumori* **103**, 44-52, doi:10.5301/tj.5000570 (2017).

15 Nassar, D., Latil, M., Boeckx, B., Lambrechts, D. & Blanpain, C. Genomic landscape of carcinogen-induced and genetically induced mouse skin squamous cell carcinoma. *Nat Med* **21**, 946-954, doi:10.1038/nm.3878 (2015).

16 Campbell, J. D. *et al.* Genomic, Pathway Network, and Immunologic Features Distinguishing Squamous Carcinomas. *Cell Rep* **23**, 194-212.e196, doi:10.1016/j.celrep.2018.03.063 (2018).
17 Hu, X. *et al.* FAT1 inhibits cell migration and invasion by affecting cellular mechanical properties in esophageal squamous cell carcinoma. *Oncol Rep* **39**, 2136-2146, doi:10.3892/or.2018.6328 (2018).
18 Hu, X. *et al.* FAT1 prevents epithelial mesenchymal transition (EMT) via MAPK/ERK signaling pathway in esophageal squamous cell cancer. *Cancer Lett* **397**, 83-93, doi:10.1016/j.canlet.2017.03.033 (2017).
19 Madan, E. *et al.* FAT1 is a novel upstream regulator of HIF1alpha and invasion of high grade glioma. *Int J Cancer* **139**, 2570-2582, doi:10.1002/ijc.30386 (2016).
20 Srivastava, C. *et al.* FAT1 modulates EMT and stemness genes expression in hypoxic glioblastoma. *Int J Cancer* **142**, 805-812, doi:10.1002/ijc.31092 (2018).
21 Pastushenko, I. *et al.* Identification of the tumour transition states occurring during EMT. *Nature* **556**, 463-468, doi:10.1038/s41586-018-0040-3 (2018).
22 Latil, M. *et al.* Cell-Type-Specific Chromatin States Differentially Prime Squamous Cell Carcinoma Tumor-Initiating Cells for Epithelial to Mesenchymal Transition. *Cell Stem Cell* **20**, 191-204.e195, doi:10.1016/j.stem.2016.10.018 (2017).
23 DuPage, M., Dooley, A. L. & Jacks, T. Conditional mouse lung cancer models using adenoviral or lentiviral delivery of Cre recombinase. *Nat Protoc* **4**, 1064-1072, doi:10.1038/nprot.2009.95 (2009).
24 Forbes, S. *et al.* COSMIC 2005. *Br J Cancer* **94**, 318-322, doi:10.1038/sj.bjc.6602928 (2006).
25 Revenco, T. *et al.* Context Dependency of Epithelial-to-Mesenchymal Transition for Metastasis. *Cell Rep* **29**, 1458-1468.e1453, doi:10.1016/j.celrep.2019.09.081 (2019).
26 Pastushenko, I. & Blanpain, C. EMT Transition States during Tumor Progression and Metastasis. *Trends Cell Biol* **29**, 212-226, doi:10.1016/j.tcb.2018.12.001 (2019).
27 Mani, S. A. *et al.* The epithelial-mesenchymal transition generates cells with properties of stem cells. *Cell* **133**, 704-715, doi:10.1016/j.cell.2008.03.027 (2008).
28 Ye, X. & Weinberg, R. A. Epithelial-Mesenchymal Plasticity: A Central Regulator of Cancer Progression. *Trends Cell Biol* **25**, 675-686, doi:10.1016/j.tcb.2015.07.012 (2015).
29 Nieto, M. A., Huang, R. Y., Jackson, R. A. & Thiery, J. P. EMT: 2016. *Cell* **166**, 21-45, doi:10.1016/j.cell.2016.06.028 (2016).
30 Lapouge, G. *et al.* Skin squamous cell carcinoma propagating cells increase with tumour progression and invasiveness. *Embo j* **31**, 4563-4575, doi:10.1038/emboj.2012.312 (2012).
31 Mehta, P., Novak, C., Raghavan, S., Ward, M. & Mehta, G. Self-Renewal and CSCs In Vitro Enrichment: Growth as Floating Spheres. *Methods Mol Biol* **1692**, 61-75, doi:10.1007/978-1-4939-7401-6_6 (2018).
32 Yang, J. *et al.* Twist, a master regulator of morphogenesis, plays an essential role in tumor metastasis. *Cell* **117**, 927-939, doi:10.1016/j.cell.2004.06.006 (2004).
33 Martin, D. *et al.* Assembly and activation of the Hippo signalome by FAT1 tumor suppressor. *Nat Commun* **9**, 2372, doi:10.1038/s41467-018-04590-1 (2018).

34 Ahmed, A. F. *et al.* FAT1 cadherin acts upstream of Hippo signalling through TAZ to regulate neuronal differentiation. *Cell Mol Life Sci* **72**, 4653-4669, doi:10.1007/s00018-015-1955-6 (2015).
35 Zanconato, F. *et al.* Genome-wide association between YAP/TAZ/TEAD and AP-1 at enhancers drives oncogenic growth. *Nat Cell Biol* **17**, 1218-1227, doi:10.1038/ncb3216 (2015).
36 Gill, M. K. *et al.* A feed forward loop enforces YAP/TAZ signaling during tumorigenesis. *Nat Commun* **9**, 3510, doi:10.1038/s41467-018-05939-2 (2018).
37 Maglic, D. *et al.* YAP-TEAD signaling promotes basal cell carcinoma development via a c-JUN/AP1 axis. *Embo j* **37**, doi:10.15252/embj.201798642 (2018).
38 Galli, G. G. *et al.* YAP Drives Growth by Controlling Transcriptional Pause Release from Dynamic Enhancers. *Mol Cell* **60**, 328-337, doi:10.1016/j.molcel.2015.09.001 (2015).
39 Liu, X. *et al.* Tead and AP1 Coordinate Transcription and Motility. *Cell Rep* **14**, 1169-1180, doi:10.1016/j.celrep.2015.12.104 (2016).
40 Shaffer, S. M. *et al.* Rare cell variability and drug-induced reprogramming as a mode of cancer drug resistance. *Nature* **546**, 431-435, doi:10.1038/nature22794 (2017).
41 Zhao, L. *et al.* YAP1 is essential for osteoclastogenesis through a TEADs-dependent mechanism. *Bone* **110**, 177-186, doi:10.1016/j.bone.2018.01.035 (2018).
42 Verfaillie, A. *et al.* Decoding the regulatory landscape of melanoma reveals TEADS as regulators of the invasive cell state. *Nat Commun* **6**, 6683, doi:10.1038/ncomms7683 (2015).
43 Boumahdi, S. *et al.* SOX2 controls tumour initiation and cancer stem-cell functions in squamous-cell carcinoma. *Nature* **511**, 246-250, doi:10.1038/nature13305 (2014).
44 Ferone, G. *et al.* SOX2 Is the Determining Oncogenic Switch in Promoting Lung Squamous Cell Carcinoma from Different Cells of Origin. *Cancer Cell* **30**, 519-532, doi:10.1016/j.ccell.2016.09.001 (2016).
45 Meng, Z. *et al.* MAP4K family kinases act in parallel to MST1/2 to activate LATS1/2 in the Hippo pathway. *Nat Commun* **6**, 8357, doi:10.1038/ncomms9357 (2015).
46 Cooper, C. D. & Lampe, P. D. Casein kinase 1 regulates connexin-43 gap junction assembly. *J Biol Chem* **277**, 44962-44968, doi:10.1074/jbc.M209427200 (2002).
47 TenBroek, E. M., Lampe, P. D., Solan, J. L., Reynhout, J. K. & Johnson, R. G. Ser364 of connexin43 and the upregulation of gap junction assembly by cAMP. *J Cell Biol* **155**, 1307-1318, doi:10.1083/jcb.200102017 (2001).
48 Solan, J. L. *et al.* Phosphorylation at S365 is a gatekeeper event that changes the structure of Cx43 and prevents down-regulation by PKC. *J Cell Biol* **179**, 1301-1309, doi:10.1083/jcb.200707060 (2007).
49 Hornbeck, P. V. *et al.* PhosphoSitePlus, 2014: mutations, PTMs and recalibrations. *Nucleic Acids Res* **43**, D512-520, doi:10.1093/nar/gku1267 (2015).
50 Lewis, C. A., Townsend, P. A. & Isacke, C. M. Ca(2+)/calmodulin-dependent protein kinase mediates the phosphorylation of CD44 required for cell migration on hyaluronan. *Biochem J* **357**, 843-850, doi:10.1042/0264-6021:3570843 (2001).

51 Huang, R. Y. *et al.* Identification of CaMKII phosphorylation sites in Connexin43 by high-resolution mass spectrometry. *J Proteome Res* **10**, 1098-1109, doi:10.1021/pr1008702 (2011).
52 Chen, C., Zhao, S., Karnad, A. & Freeman, J. W. The biology and role of CD44 in cancer progression: therapeutic implications. *J Hematol Oncol* **11**, 64, doi:10.1186/s13045-018-0605-5 (2018).
53 Jolly, M. K. *et al.* Interconnected feedback loops among ESRP1, HAS2, and CD44 regulate epithelial-mesenchymal plasticity in cancer. *APL Bioeng* **2**, 031908, doi:10.1063/1.5024874 (2018).
54 Chellaiah, M. A., Biswas, R. S., Rittling, S. R., Denhardt, D. T. & Hruska, K. A. Rho-dependent Rho kinase activation increases CD44 surface expression and bone resorption in osteoclasts. *J Biol Chem* **278**, 29086-29097, doi:10.1074/jbc.M211074200 (2003).
55 Nam, K., Oh, S., Lee, K. M., Yoo, S. A. & Shin, I. CD44 regulates cell proliferation, migration, and invasion via modulation of c-Src transcription in human breast cancer cells. *Cell Signal* **27**, 1882-1894, doi:10.1016/j.cellsig.2015.05.002 (2015).
56 Lee, J. L., Wang, M. J., Sudhir, P. R. & Chen, J. Y. CD44 engagement promotes matrix-derived survival through the CD44-SRC-integrin axis in lipid rafts. *Mol Cell Biol* **28**, 5710-5723, doi:10.1128/mcb.00186-08 (2008).
57 Bourguignon, L. Y., Zhu, H., Shao, L. & Chen, Y. W. CD44 interaction with c-Src kinase promotes cortactin-mediated cytoskeleton function and hyaluronic acid-dependent ovarian tumor cell migration. *J Biol Chem* **276**, 7327-7336, doi:10.1074/jbc.M006498200 (2001).
58 Gollner, S. *et al.* Loss of the histone methyltransferase EZH2 induces resistance to multiple drugs in acute myeloid leukemia. *Nat Med* **23**, 69-78, doi:10.1038/nm.4247 (2017).
59 Avgustinova, A. & Benitah, S. A. Epigenetic control of adult stem cell function. *Nat Rev Mol Cell Biol* **17**, 643-658, doi:10.1038/nrm.2016.76 (2016).
60 Panciera, T., Azzolin, L., Cordenonsi, M. & Piccolo, S. Mechanobiology of YAP and TAZ in physiology and disease. *Nat Rev Mol Cell Biol* **18**, 758-770, doi:10.1038/nrm.2017.87 (2017).
61 Machiels, J. P. *et al.* Afatinib versus methotrexate as second-line treatment in patients with recurrent or metastatic squamous-cell carcinoma of the head and neck progressing on or after platinum-based therapy (LUX-Head & Neck 1): an open-label, randomised phase 3 trial. *Lancet Oncol* **16**, 583-594, doi:10.1016/s1470-2045(15)70124-5 (2015).
62 Lai, W. V. *et al.* Afatinib in patients with metastatic or recurrent HER2-mutant lung cancers: a retrospective international multicentre study. *Eur J Cancer* **109**, 28-35, doi:10.1016/j.ejca.2018.11.030 (2019).
63 Planchard, D. *et al.* Dabrafenib plus trametinib in patients with previously untreated BRAF(V600E)-mutant metastatic non-small-cell lung cancer: an open-label, phase 2 trial. *Lancet Oncol* **18**, 1307-1316, doi:10.1016/s1470-2045(17)30679-4 (2017).
64 Ng, P. C. & Henikoff, S. SIFT: Predicting amino acid changes that affect protein function. *Nucleic Acids Res* **31**, 3812-3814, doi:10.1093/nar/gkg509 (2003).
65 Adzhubei, I., Jordan, D. M. & Sunyaev, S. R. Predicting functional effect of human missense mutations using PolyPhen-2. *Curr Protoc Hum Genet* **Chapter 7**, Unit7.20, doi:10.1002/0471142905.hg0720s76 (2013).

66 Ciriello, G., Cerami, E., Sander, C. & Schultz, N. Mutual exclusivity analysis identifies oncogenic network modules. *Genome Res* **22**, 398-406, doi:10.1101/gr.125567.111 (2012).

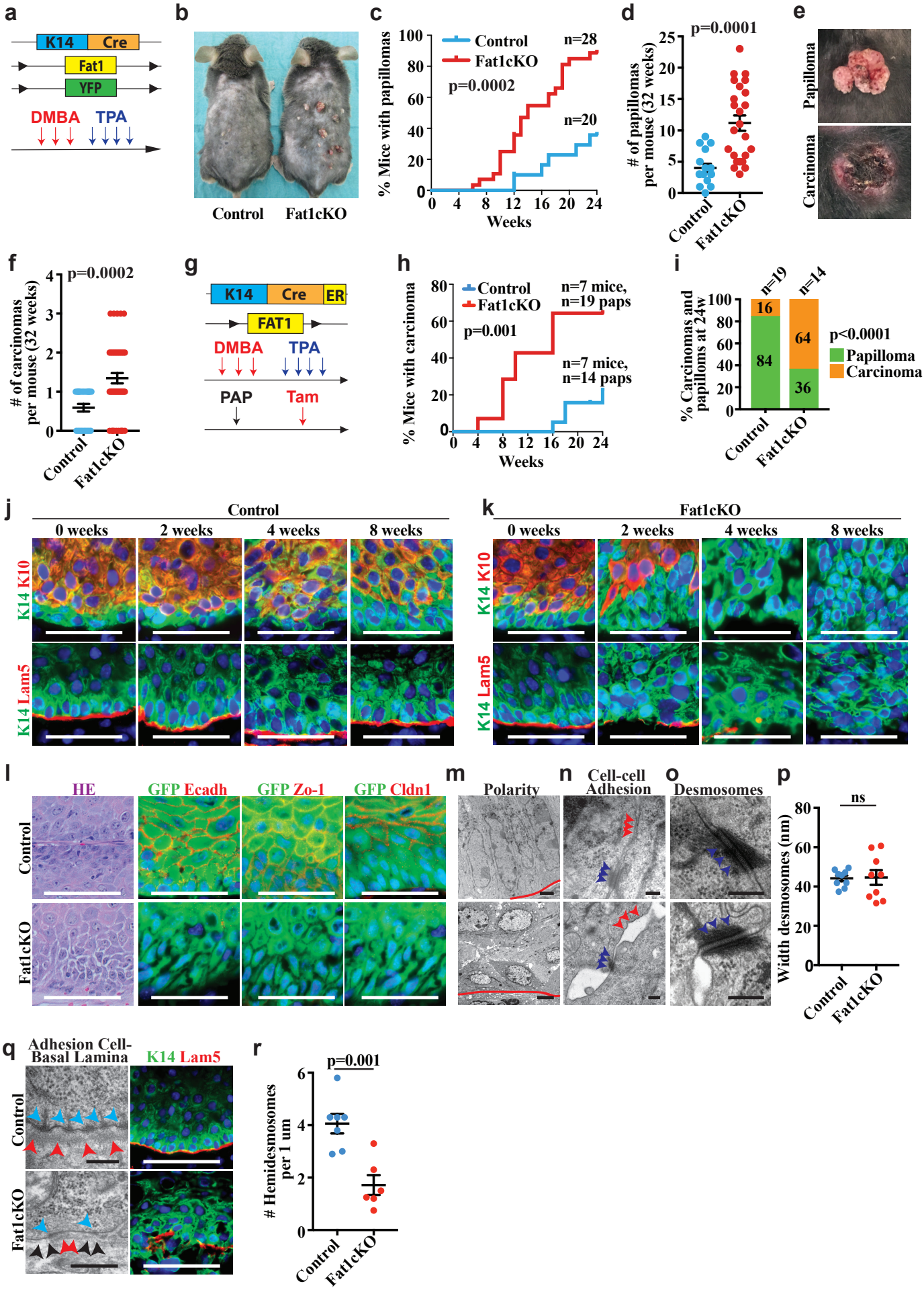
a
K14
Cre
Fat1
YFP
DMBA
TPA
b
Control
Fat1cKO
c
% Mice with papillomas
Control
Fat1cKO
n=28
n=20
p=0.0002
Weeks
d
p=0.0001
# of papillomas per mouse (32 weeks)
Control
Fat1cKO
e
Papilloma
Carcinoma
f
p=0.0002
# of carcinomas per mouse (32 weeks)
Control
Fat1cKO
g
K14
Cre
ER
FAT1
DMBA
TPA
PAP
Tam
h
% Mice with carcinoma
Control
Fat1cKO
n=7 mice, n=19 paps
n=7 mice, n=14 paps
p=0.001
Weeks
i
n=19
n=14
% Carcinomas and papillomas at 24w
16
84
64
36
p<0.0001
Papilloma
Carcinoma
Control
Fat1cKO
j
Control
0 weeks
2 weeks
4 weeks
8 weeks
K14 K10
K14 Lam5
k
Fat1cKO
0 weeks
2 weeks
4 weeks
8 weeks
K14 K10
K14 Lam5
l
HE
GFP Ecadh
GFP Zo-1
GFP Cldn1
Control
Fat1cKO
m
Polarity
n
Cell-cell Adhesion
o
Desmosomes
p
ns
Width desmosomes (nm)
Control
Fat1cKO
q
Adhesion Cell-Basal Lamina
K14 Lam5
Control
Fat1cKO
r
p=0.001
# Hemidesmosomes per 1 um
Control
Fat1cKO

Figure 1

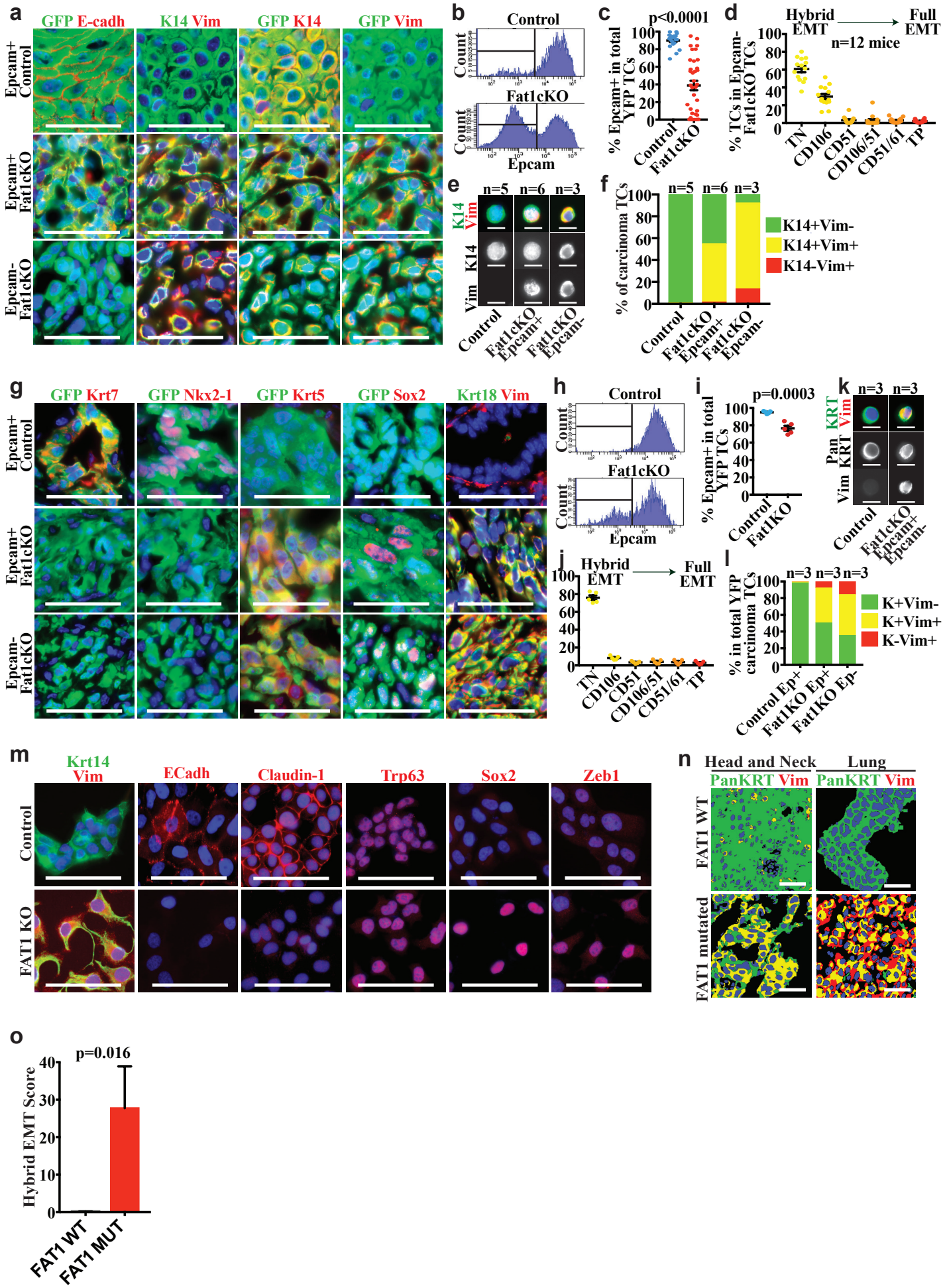
a
GFP E-cadh
K14 Vim
GFP K14
GFP Vim
Epcam+ Control
Epcam+ Fat1cKO
Epcam- Fat1cKO
b
Control
Fat1cKO
Count
Epcam
c
p<0.0001
% Epcam+ in total YFP TCs
Control
Fat1cKO
d
Hybrid EMT
Full EMT
n=12 mice
% TCs in Epcam- Fat1cKO TCs
TN
CD106
CD51
CD106/51
CD51/61
TP
e
n=5
n=6
n=3
K14 Vim
K14
Vim
Control
Fat1cKO Epcam+
Fat1cKO Epcam-
f
% of carcinoma TCs
K14+Vim-
K14+Vim+
K14-Vim+
g
GFP Krt7
GFP Nkx2-1
GFP Krt5
GFP Sox2
Krt18 Vim
h
i
p=0.0003
k
KRT Vim
Pan KRT Vim
j
l
% in total YFP carcinoma TCs
K+Vim-
K+Vim+
K-Vim+
Control Ep+
Fat1KO Ep+
Fat1KO Ep-
m
Krt14 Vim
ECadh
Claudin-1
Trp63
Sox2
Zeb1
Control
FAT1 KO
n
Head and Neck
Lung
PanKRT Vim
FAT1 WT
FAT1 mutated
o
p=0.016
Hybrid EMT Score
FAT1 WT
FAT1 MUT

Figure 2

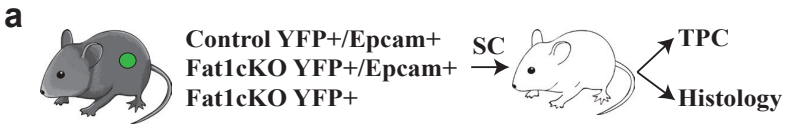

Number grafted cells	Control Epcam+	Fat1cKO Epcam+	Fat1cKO Total YFP+
10000	7/9 (n=3)	12/12 (n=4)	15/15 (n=4)
1000	2/9 (n=3)	9/12 (n=4)	15/15 (n=4)
100	1/9 (n=3)	2/12 (n=4)	8/15 (n=4)
10	1/9 (n=3)	2/16 (n=4)	3/30 (n=4)
TPC frequency	1/4117 (9786-2326)	1/578 (310-1076)	1/121 (66-220)

p=4.72e-06 (Chisq=20.9, DF=1)

p=4.72e-06 (Chisq=70.5, DF=1)

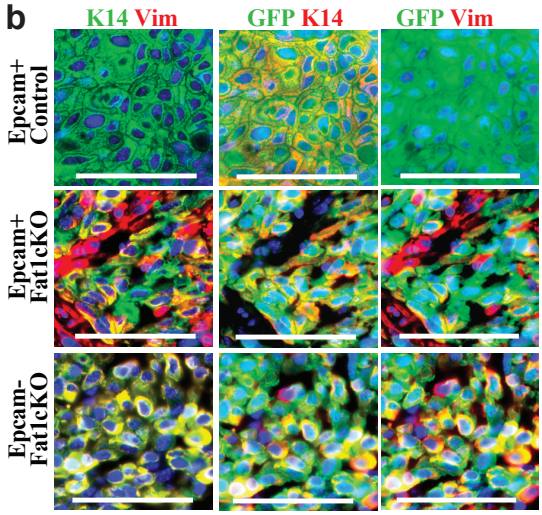

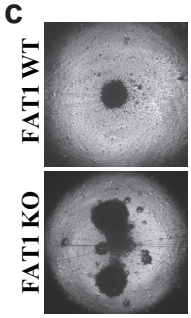

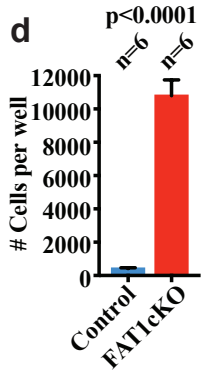

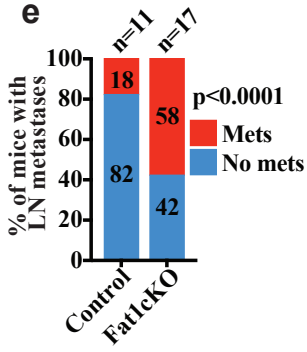

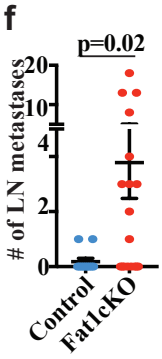

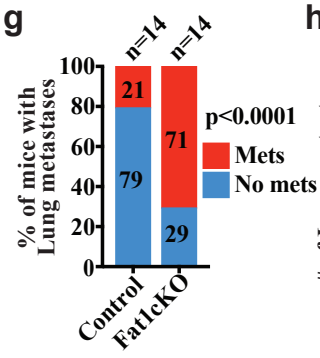

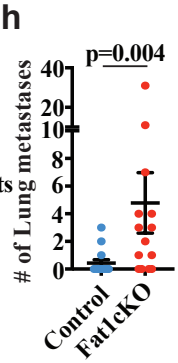

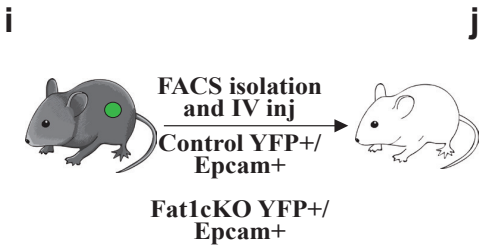

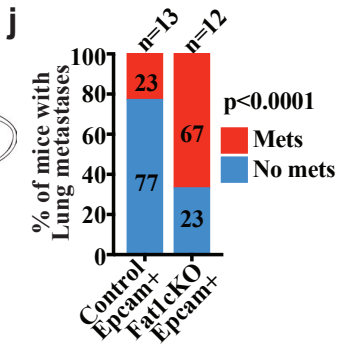

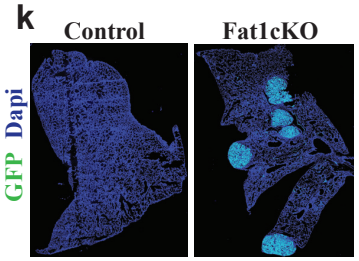

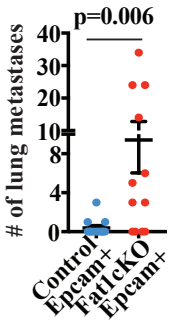

Figure 3

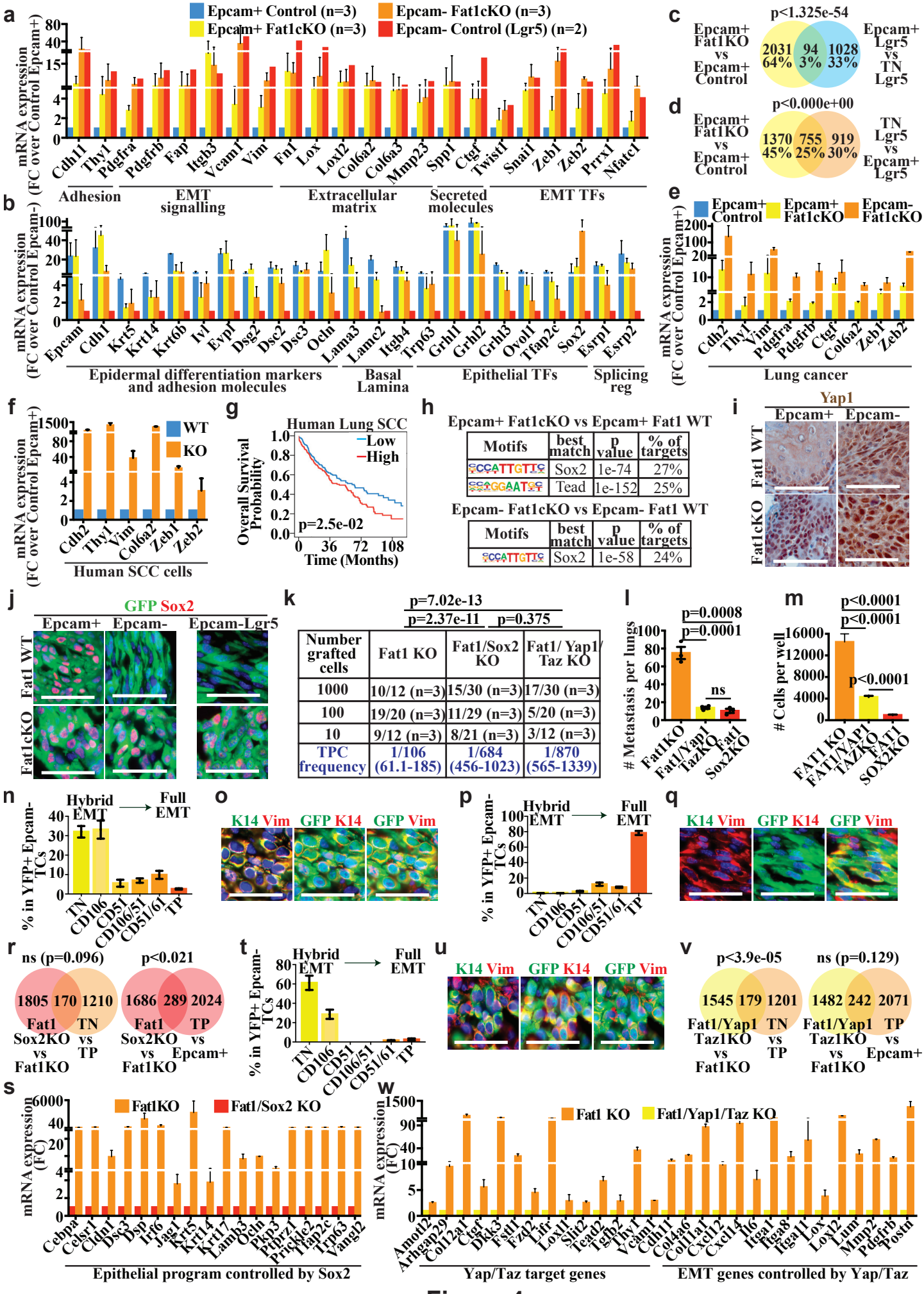
a
Epcam+ Control (n=3)
Epcam+ Fat1cKO (n=3)
Epcam- Fat1cKO (n=3)
Epcam- Control (Lgr5) (n=2)
mRNA expression (FC over Control Epcam+)
Cdh11 Thy1 Pdgfra Pdgfrb Fap Itgb3 Vcam1 Vim Fn1 Lox Loxl2 Col6a2 Col6a3 Mmp23 Spp1 Ctgf Twist1 Snai1 Zeb1 Zeb2 Prrx1 Nfatc1
Adhesion
EMT signalling
Extracellular matrix
Secreted molecules
EMT TFs
b
mRNA expression (FC over Control Epcam-)
Epcam Cdh1 Krt5 Krt14 Krt6b Ivl Evpl Dsg2 Dsc2 Dsc3 Ocln Lama3 Lamc2 Itgb4 Trp63 Grhl1 Grhl2 Grhl3 Ovol1 Tfap2c Sox2 Esrp1 Esrp2
Epidermal differentiation markers and adhesion molecules
Basal Lamina
Epithelial TFs
Splicing reg
c
p<1.325e-54
Epcam+ Fat1KO vs Epcam+ Control
2031 64%
94 3%
1028 33%
Epcam+ Lgr5 vs TN Lgr5
d
p<0.000e+00
Epcam+ Fat1KO vs Epcam+ Control
1370 45%
755 25%
919 30%
TN Lgr5 vs Epcam+ Lgr5
e
Epcam+ Control
Epcam+ Fat1cKO
Epcam- Fat1cKO
mRNA expression (FC over Control Epcam+)
Cdh2 Thy1 Vim Pdgfra Pdgfrb Ctgf Col6a2 Zeb1 Zeb2
Lung cancer
f
WT
KO
mRNA expression (FC over Control Epcam+)
Cdh2 Thy1 Vim Col6a2 Zeb1 Zeb2
Human SCC cells
g
Human Lung SCC
Low
High
Overall Survival Probability
p=2.5e-02
Time (Months)
h
Epcam+ Fat1cKO vs Epcam+ Fat1 WT
Motifs | best match | p value | % of targets
Sox2 | 1e-74 | 27%
Tead | 1e-152 | 25%
Epcam- Fat1cKO vs Epcam- Fat1 WT
Motifs | best match | p value | % of targets
Sox2 | 1e-58 | 24%
i
Yap1
Epcam+
Epcam-
Fat1 WT
Fat1cKO
j
GFP Sox2
Epcam+
Epcam-
Epcam-Lgr5
Fat1 WT
Fat1cKO
k
p=7.02e-13
p=2.37e-11
p=0.375
Number grafted cells | Fat1 KO | Fat1/Sox2 KO | Fat1/ Yap1/ Taz KO
1000 | 10/12 (n=3) | 15/30 (n=3) | 17/30 (n=3)
100 | 19/20 (n=3) | 11/29 (n=3) | 5/20 (n=3)
10 | 9/12 (n=3) | 8/21 (n=3) | 3/12 (n=3)
TPC frequency | 1/106 (61.1-185) | 1/684 (456-1023) | 1/870 (565-1339)
l
p=0.0008
p=0.0001
ns
Metastasis per lungs
Fat1KO Fat1/Yap1 TazKO Fat1 Sox2KO
m
p<0.0001
p<0.0001
p<0.0001
Cells per well
FAT1 KO FAT1/YAP1 TAZKO FAT1 SOX2KO
n
Hybrid EMT
Full EMT
% in YFP+ Epcam- TCs
TN CD106 CD51 CD106/51 CD51/61 TP
o
K14 Vim
GFP K14
GFP Vim
p
Hybrid EMT
Full EMT
% in YFP+ Epcam- TCs
TN CD106 CD51 CD106/51 CD51/61 TP
q
K14 Vim
GFP K14
GFP Vim
r
ns (p=0.096)
1805 Fat1 Sox2KO vs Fat1KO
170 TN vs TP
1210
p<0.021
1686 Fat1 Sox2KO vs Fat1KO
289 TP vs Epcam+ Fat1KO
2024
t
Hybrid EMT
Full EMT
% in YFP+ Epcam- TCs
TN CD106 CD51 CD106/51 CD51/61 TP
u
K14 Vim
GFP K14
GFP Vim
v
p<3.9e-05
1545 Fat1/Yap1 Taz1KO vs Fat1KO
179 TN vs TP
1201
ns (p=0.129)
1482 Fat1/Yap1 Taz1KO vs Fat1KO
242 TP vs Epcam+ Fat1KO
2071
s
Fat1KO
Fat1/Sox2 KO
mRNA expression (FC)
Cebpa Celsr1 Cldn1 Dsc3 Dsp Irf6 Jag1 Krt5 Krt14 Krt17 Lamb3 Odn Pkp3 Ptprz1 Prickle2 Tfap2c Trp63 Vangl2
Epithelial program controlled by Sox2
w
Fat1 KO
Fat1/Yap1/Taz KO
mRNA expression (FC)
Amotl2 Arhgap29 Col12a1 Ctgf Dkk3 Fstl1 Fzd2 Lifr Loxl1 Slit2 Tead2 Tgfb2 Thy1 Vcam1 Cdh11 Col4a6 Col11a1 Cxcl12 Cxcl14 Il6 Itga1 Itga8 Itga11 Lox Loxl2 Lum Mmp2 Pdgfrb Postn
Yap/Taz target genes
EMT genes controlled by Yap/Taz

Figure 4

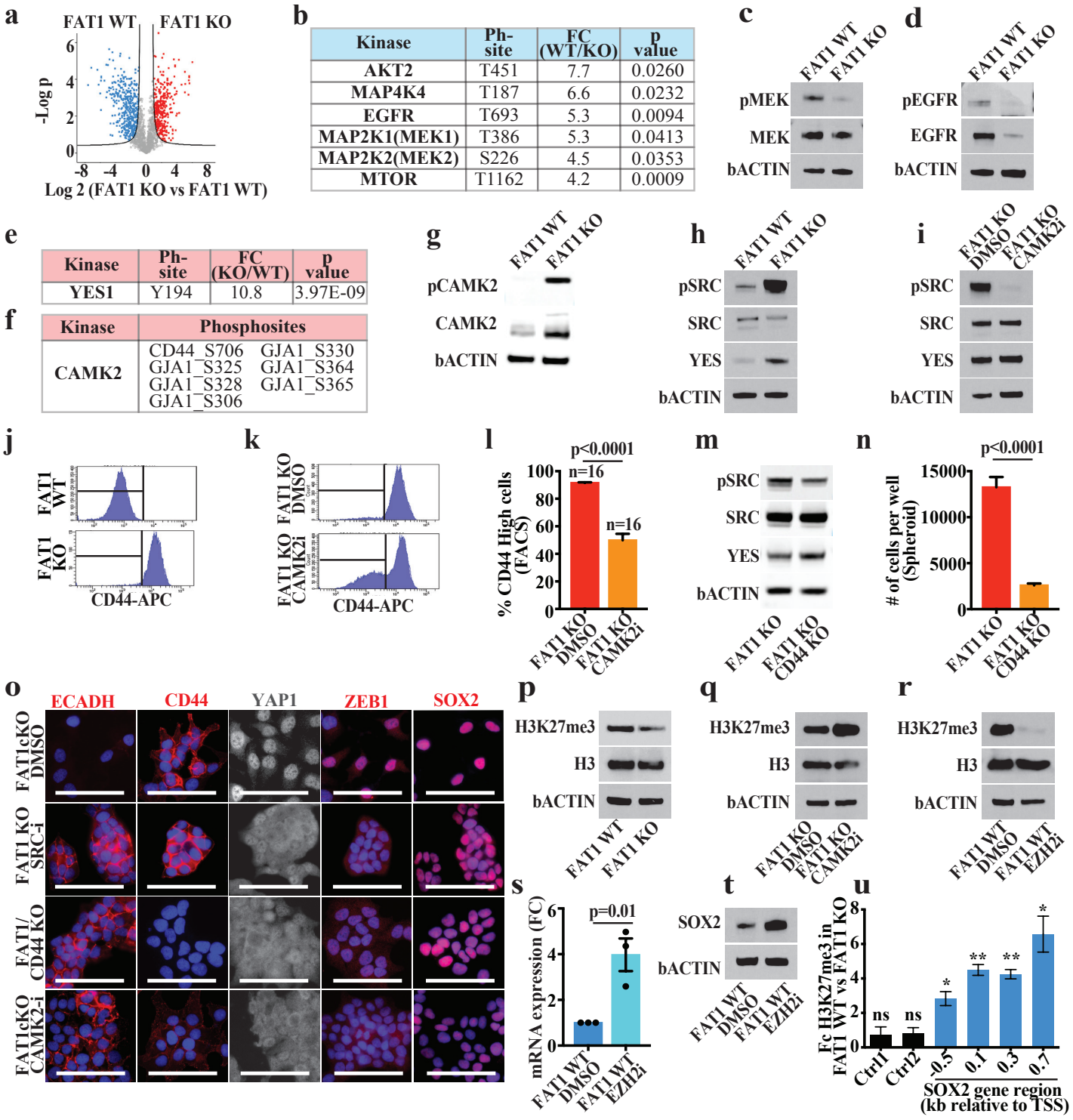

Kinase	Ph-site	FC (WT/KO)	p value
AKT2	T451	7.7	0.0260
MAP4K4	T187	6.6	0.0232
EGFR	T693	5.3	0.0094
MAP2K1(MEK1)	T386	5.3	0.0413
MAP2K2(MEK2)	S226	4.5	0.0353
MTOR	T1162	4.2	0.0009

Kinase	Ph-site	FC (KO/WT)	p value
YES1	Y194	10.8	3.97E-09

Kinase	Phosphosites
CAMK2	CD44_S706 GJA1_S330 GJA1_S325 GJA1_S364 GJA1_S328 GJA1_S365 GJA1_S306

Drug	FAT1 WT #	FAT1 WT pIC50	FAT1 WT SEM	FAT1 KO #	FAT1 KO pIC50	FAT1 KO SEM	p-value
EGFRi (Afatinib)	3	6.92	0.11	3	5.67	0.15	0.0232
MEKi (Trametinib)	3	6.97	0.17	3	4.62	0.05	0.0002
SRCi (Dasatinib)	3	6.15	0.18	3	7.50	0.14	0.0041
SRCi (Saracatinib)	3	5.71	0.09	4	6.58	0.18	0.0108
CAMK2i (KN93)	2	3.69	0.04	2	4.40	0.09	0.0216

Figure 5